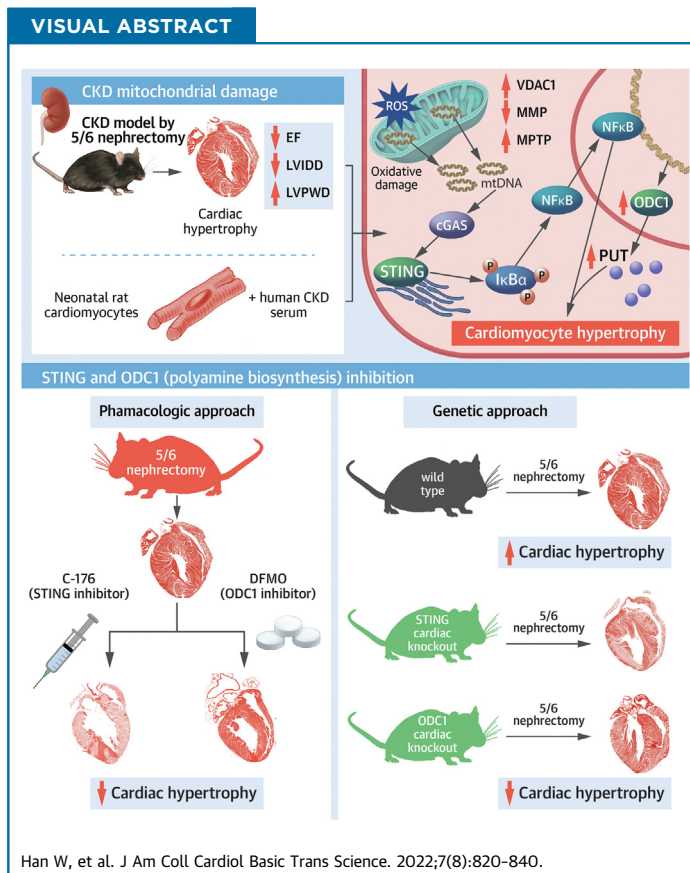


ORIGINAL RESEARCH - PRECLINICAL

# Targeting Myocardial Mitochondria-STING-Polyamine Axis Prevents Cardiac Hypertrophy in Chronic Kidney Disease



Wenhao Han, MD,<sup>a,\*</sup> Changhong Du, PhD,<sup>b,\*</sup> Yingguo Zhu, MS,<sup>a</sup> Li Ran, MS,<sup>a</sup> Yue Wang, MD,<sup>a</sup> Jiachuan Xiong, MD,<sup>a</sup> Yiding Wu, PhD,<sup>b</sup> Qigang Lan, MS,<sup>a</sup> Yaqin Wang, MS,<sup>a</sup> Litng Wang, MS,<sup>c</sup> Junping Wang, PhD,<sup>b</sup> Ke Yang, PhD,<sup>a</sup> Jinghong Zhao, MD, PhD<sup>a</sup>



## HIGHLIGHTS

- Mitochondrial damage is early and prominent in cardiomyocytes under CKD milieu.
- Mitochondrial damage stimulates myocardial STING-NFκB pathway to drive hypertrophy.
- NFκB transactivates ODC1-PUT metabolic flux in cardiomyocytes.
- ODC1-PUT metabolic flux is required for STING/NFκB-driven cardiac hypertrophy.
- Targeting mitochondria-STING-ODC1 axis prevents cardiac hypertrophy in CKD.

From the <sup>a</sup>Department of Nephrology, the Key Laboratory for the Prevention and Treatment of Chronic Kidney Disease of Chongqing, Chongqing Clinical Research Center of Kidney and Urology Diseases, Xinqiao Hospital, Army Medical University (Third Military Medical University), Chongqing, China; <sup>b</sup>State Key Laboratory of Trauma, Burns and Combined Injury, Institute of Combined Injury, Chongqing Engineering Research Center for Nanomedicine, College of Preventive Medicine, Army Medical University (Third Military Medical University), Chongqing, China; and the <sup>c</sup>Biomedical Analysis Center, Army Medical University (Third Military Medical University), Chongqing, China. \*Drs Han and Du contributed equally to this work.

## ABSTRACT

Chronic kidney disease (CKD) is well recognized as a distinct contributor to cardiac hypertrophy, while the underlying mechanism remains incompletely understood. Here, the authors show that myocardial mitochondrial oxidative damage is early and prominent in CKD and distinctively stimulates the STING-NFκB pathway by releasing mitochondrial DNA to drive cardiac hypertrophy. Furthermore, the authors reveal that ornithine decarboxylase (ODC1)-putrescine metabolic flux is transactivated by NFκB and is required for the STING-NFκB pathway to drive cardiac hypertrophy. Finally, genetic or pharmacologic inhibition of the myocardial mitochondria-STING-NFκB-ODC1 axis significantly prevents CKD-associated cardiac hypertrophy. Therefore, targeting the myocardial mitochondria-STING-NFκB-ODC1 axis is a promising therapeutic strategy for cardiac hypertrophy in patients with CKD. (J Am Coll Cardiol Basic Trans Science 2022;7:820-840) © 2022 The Authors. Published by Elsevier on behalf of the American College of Cardiology Foundation. This is an open access article under the CC BY-NC-ND license (<http://creativecommons.org/licenses/by-nc-nd/4.0/>).

Cardiac hypertrophy is one of the most prevalent markers of cardiovascular disease among patients with chronic kidney disease (CKD) and is strongly associated with increased risks for arrhythmias, dilated cardiomyopathy, heart failure, and sudden cardiac death.<sup>1,2</sup> Unfortunately, CKD-associated cardiac hypertrophy remains intractable because of the incomplete understanding of its pathogenesis. Along with the progression of CKD, the deficiency of kidney-derived secretory factors and the accumulation of large amounts of uremic toxins build the CKD milieu. Currently, substantial evidence has shown that the components of the CKD milieu are distinct contributors to cardiac hypertrophy in CKD.<sup>3-7</sup> However, few studies have deeply defined the key molecules that respond to the whole CKD milieu and drive the cardiac hypertrophic response. Consequently, this knowledge gap is a key hindrance for the identification of new and effective therapeutic targets to control this growing epidemic.

Cardiac hypertrophy always accompanies the remodeling of cardiac metabolic networks that results in both adenosine triphosphate (ATP)-producing and non-ATP-producing effects.<sup>8</sup> ATP-producing metabolic pathways are necessary to sustain optimal cardiac function and thus get most of the attention in studies of cardiac pathophysiology. Mitochondria are particularly rich in cardiomyocytes and serve a key role in ATP generation via oxidative phosphorylation. Therefore, perturbations of mitochondrial homeostasis are frequently reported in cardiac hypertrophy.<sup>9</sup> Nevertheless, recent studies suggest that

mitochondrial perturbations are not simply a consequence of cardiac hypertrophy but rather directly contribute to the development of cardiac hypertrophy.<sup>10-12</sup> However, how mitochondria orchestrate the cardiac hypertrophic response to hypertrophic stimuli remains unclear. Meanwhile, myocardial mitochondrial homeostasis in CKD and its pathogenic role are largely unknown.

In contrast, though always undervalued, non-ATP-producing metabolic pathways actually generate biosynthetic intermediates to support the enlargement of a cell.<sup>13</sup> One of the most representative non-ATP-producing metabolic pathways that are essential for cell growth is polyamine metabolism, which is a branch of arginine metabolism and produces polyamines including spermidine, spermine, and their precursor putrescine (PUT).<sup>14</sup> Particularly, it is well documented that polyamine contents are always concomitantly increased with cardiac mass in response to most hypertrophic stimuli.<sup>15-17</sup> Nevertheless, the distinct actions of polyamines in cardiac pathophysiology, including CKD-associated cardiac hypertrophy are not yet defined. In addition, it remains unclear that whether mitochondrial perturbations and polyamine metabolism are independent or cooperative in the pathogenesis of cardiac hypertrophy.

In this study, we reveal that mitochondrial oxidative damage is early and prominent in cardiomyocytes in a CKD milieu. Mitochondrial oxidative damage-induced and voltage-dependent anion channel 1 (VDAC1)-mediated mitochondrial

## ABBREVIATIONS AND ACRONYMS

- ATP** = adenosine triphosphate
- CKD** = chronic kidney disease
- LV** = left ventricular
- MOMP** = mitochondrial outer membrane permeabilization
- MPTP** = mitochondrial permeability transition pore
- mtDNA** = mitochondrial DNA
- NRCM** = primary neonatal rat cardiomyocyte
- ODC1** = ornithine decarboxylase
- PUT** = putrescine
- ROS** = reactive oxygen species
- siRNA** = small interfering RNA
- VDAC1** = voltage-dependent anion channel 1

The authors attest they are in compliance with human studies committees and animal welfare regulations of the authors' institutions and Food and Drug Administration guidelines, including patient consent where appropriate. For more information, visit the [Author Center](#).

Manuscript received January 26, 2022; revised manuscript received March 24, 2022, accepted March 24, 2022.

outer membrane permeabilization (MOMP) triggers mitochondrial DNA (mtDNA) release, which initiates CKD-induced cardiac hypertrophic response through stimulating the STING-NF $\kappa$ B pathway. Furthermore, NF $\kappa$ B-transactivated ornithine decarboxylase (ODC1)-PUT metabolic flux acts as an indispensable contributor for STING-NF $\kappa$ B pathway-driven cardiac hypertrophic program. Targeting the myocardial mitochondria-STING-polyamine axis holds promise for the treatment of cardiac hypertrophy in patients with CKD.

## METHODS

**ANIMALS.** MYH6-Cre/Esr1 (*Myh6*<sup>CreER</sup>) mice, C57BL/6-Odc1<sup>em1(flox)Smoc</sup> (*Odc1*<sup>flox/flox</sup>) mice, and B6;129S-Tmem173<sup>tm1(flox)Smoc</sup> (*Sting*<sup>flox/flox</sup>) mice were purchased from Shanghai Model Organisms Center. C57BL/6N-Mb21d1<sup>tm1cyagen</sup> (*cGAS*<sup>-/-</sup>) mice and C57BL/6N-Tmem173<sup>tm1cyagen</sup> (*Sting*<sup>-/-</sup>) mice were purchased from Cyagen Biosciences. *Odc1*<sup>cko</sup> and *Sting*<sup>cko</sup> mice were obtained by crossing *Myh6*<sup>CreER</sup> mice with *Odc1*<sup>flox/flox</sup> mice and *Sting*<sup>flox/flox</sup> mice, respectively. Normal C57BL/6 male mice were purchased from Beijing HFK Bioscience. The CKD mouse model was created as previously described.<sup>7</sup> Briefly, male C57BL/6 mice at 8 weeks of age were first inflicted with two-thirds electrocoagulation of the right renal cortex and then underwent left total nephrectomy 2 weeks later.

To pharmacologically inhibit ODC1, mice were administered difluoromethylornithine (MedChem Express) at 2% final concentration in their drinking water. For VBIT-4 (Selleck Chemicals) administration, mice were orally treated with VBIT-4 in drinking water for 5 consecutive weeks. For preparation of the VBIT-4, drinking water was firstly titrated to pH 4 with hydrogen chloride (HCl). Then, VBIT-4 dissolved in dimethyl sulfoxide was added in a dropwise manner into the acidic water to reach a final concentration of 0.3 mg mL<sup>-1</sup>. For PUT (MedChem Express) supplementation, mice were given PUT in their drinking water at 2 mM. As one mouse consumes about 60 mL kg<sup>-1</sup> water per day,<sup>18</sup> the daily doses of difluoromethylornithine, VBIT-4, and PUT were approximately 1.2 g kg<sup>-1</sup>, 20 mg kg<sup>-1</sup>, and 10.58 mg kg<sup>-1</sup>, respectively. To pharmacologically inhibit NF $\kappa$ B, mice were given ammonium pyrrolidinedithiocarbamate (MedChem Express), which is a pre-clinically available oral drug, in their drinking water at a dose of 100 mg kg<sup>-1</sup>. Fluid consumption was verified, and the drinking water was replaced on a daily basis. C-176 (MedChem Express) was reconstituted in dimethyl sulfoxide at 10 mg mL<sup>-1</sup> and

diluted in 5% Tween-80 (Sigma-Aldrich) and 5% PEG-400 (Sangon Biotech). To pharmacologically inhibit STING in vivo, mice were treated with a dose of 4 mg kg<sup>-1</sup> intraperitoneally every other day.

All mice were age matched, male, and syngeneic in a C57BL/6 background and were housed, bred, and maintained under specific pathogen-free conditions. All experimental procedures were approved by the Animal Care and Use Committee of the Army Medical University (Third Military Medical University).

**HUMAN SAMPLES.** Uremic and healthy sera were collected from patients with stage 5 CKD undergoing conservative treatment in the Physical Examination Department of Xinqiao Hospital for sex- and age-matched subjects, respectively. Ten milliliters whole blood was collected, and serum was separated by centrifuging at 1,000 rpm for 10 minutes at room temperature. The serum was placed in 56°C water for 30 minutes, then centrifuged at 3,000 rpm for another 10 minutes. The supernatant was collected and filtered with a cell strainer (0.22  $\mu$ m; Merck Millipore). The exclusion criteria included inflammatory and autoimmune-associated disease, hypohepatia, polycystic kidney disease, renal cancer, pregnancy, and diabetes. Blood urea nitrogen, creatinine, and glucose were assayed in all patients, and normal sera were excluded if creatinine was >1.0 mg dL<sup>-1</sup>. The study protocol was approved by the Ethics Committee of Xinqiao Hospital, and the study was carried out in accordance with the Declaration of Helsinki.

**CELL CULTURE.** Primary neonatal rat cardiomyocytes (NRCMs) were isolated and cultured as previously reported.<sup>7</sup> Briefly, the left ventricles of 1-day-old neonatal Sprague-Dawley rats (Beijing HFK Bioscience) were harvested and digested with 1.25% trypsin (Thermo Fisher Scientific) at room temperature, then incubated with 0.08% collagenase II (Solarbio Life Sciences) at 37°C. Cells were filtered with a cell strainer (70  $\mu$ m; BD Falcon). The suspension was centrifuged at 1,500 rpm for 10 minutes. After being washed with PBS, the precipitate was resuspended in Dulbecco's modified Eagle's medium-high glucose (Gibco) with 15% fetal bovine serum (Gibco) and 0.1 mM bromodeoxyuridine for 48 hours. Finally, NRCMs were cultured in Dulbecco's modified Eagle's medium-high glucose supplemented with 20% healthy or CKD serum and 1% (vol/vol) penicillin/streptomycin for 48 hours. To inhibit ODC1, cells were pretreated with 0.5 mM difluoromethylornithine for 24 hours. To block MOMP, cells were pretreated with 10  $\mu$ M VBIT-4 for 1 hour. To inhibit BAX, cells were

pretreated with 2  $\mu\text{M}$  BAI1 (Selleck Chemicals) for 24 hours. To scavenge reactive oxygen species (ROS), cells were pretreated with 5 mM *N*-acetylcysteine (Sigma-Aldrich) for 1 hour.

**ECHOCARDIOGRAPHY.** Mice were lightly anesthetized with 0.5% isoflurane and 99.5%  $\text{O}_2$  and imaged in the supine position using a high-resolution micro-imaging system equipped with a 30-MHz linear-array transducer (Vevo 2100 Imaging System, VisualSonics). Then, left ventricular (LV) internal diameter at diastole, LV internal diameter at systole, and LV posterior wall thickness at end-diastole were measured. The percentage of fractional shortening was calculated using the equation:  $100\% \times [(\text{LV internal diameter at diastole} - \text{LV internal diameter at systole}) / \text{LV internal diameter at diastole}]$ . The ejection fraction and LV mass were recorded using the Vevo 2100 Imaging System. LV mass/tibial length ratio was calculated. All measures were averaged from 5 to 7 consecutive cardiac cycles under stable conditions.

**MYOCARDIAL AND INTRACELLULAR ROS ANALYSIS.** Fresh frozen sections of myocardium were incubated with 10  $\mu\text{M}$  dihydroethidium (Thermo Fisher Scientific) in a humidified chamber protected from light for 0.5 hours at 37 °C and then photographed under a fluorescence microscope (Olympus Optical). The cells were incubated with 10  $\mu\text{M}$  2',7'-dichlorodihydrofluorescein diacetate (Sigma-Aldrich) for 30 minutes at 37°C, protected from light, followed by the detection of ROS in a microplate reader (SpectraMax M5, Molecular Devices) and microscope (Olympus Optical).

**MYOCARDIAL MITOCHONDRIAL FUNCTION MEASUREMENT IN VIVO.** Myocardial mitochondria were isolated using a Tissue Mitochondria Isolation Kit (Beyotime) following the manufacturer's instructions. Briefly, myocardia were homogenized on ice, followed by centrifugation at 600g for 5 minutes at 4°C. The supernatants were collected and centrifuged at 11,000g for 10 minutes at 4°C to pellet mitochondria. Myocardial mitochondrial membrane potential was determined using 5,5',6,6'-tetrachloro-1,1',3,3'-tetraethylbenzimidazolcarbocyanine iodide dye. Briefly, mitochondria were stained at 37°C for 30 minutes, and then red/green fluorescent intensity was determined using a fluorescent microplate reader. Mitochondrial membrane potential was calculated by determining the red/green fluorescence ratio. To measure myocardial MOMP,  $\text{CaCl}_2$  (150  $\mu\text{M}$ ) was added to freshly isolated mitochondrial suspension, and absorbance changes at 540 nm were monitored every 16 seconds for 15 minutes. MOMP ( $\Delta A$ ) was evaluated by calculating the total decrease in

absorbance from 0 minutes ( $A_0$ ) to 15 minutes ( $A_{15}$ ) ( $\Delta A = A_0 - A_{15}$ ). To measure mitochondrial respiratory function, the activity of mitochondrial complex IV, the terminal electron acceptor in the mitochondrial electron transport chain, was determined using a MitoCheck Complex IV Activity Assay Kit (Cayman Chemical) following the manufacturer's instructions. Absorbance was measured at 550 nm for 15 minutes using a microplate reader.

#### MYOCARDIAL MITOCHONDRIAL FUNCTION MEASUREMENT IN VITRO.

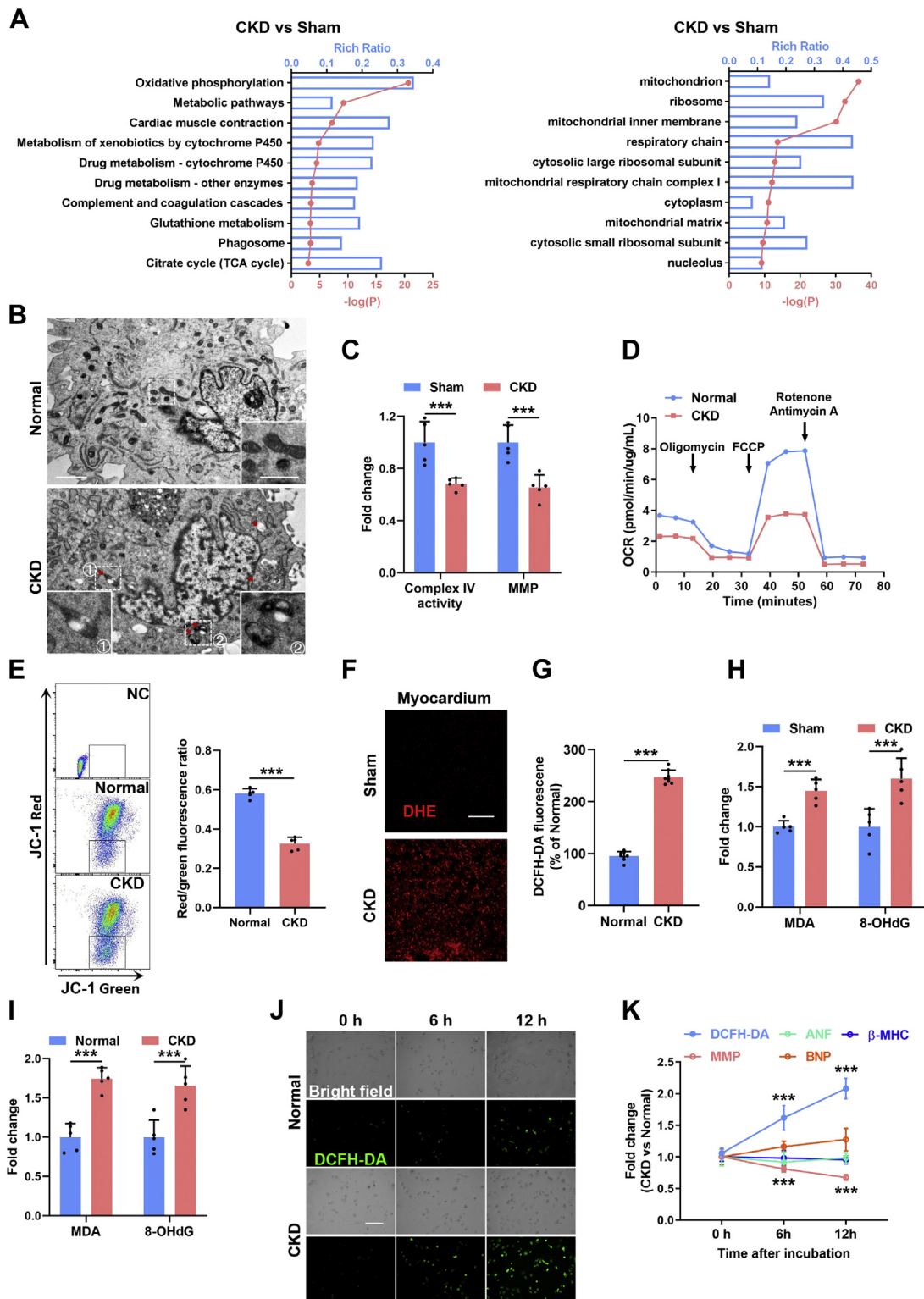
To measure mitochondrial membrane potential in vitro, the suspended NRCMs were stained with 5,5',6,6'-tetrachloro-1,1',3,3'-tetraethylbenzimidazolcarbocyanine iodide at 37°C for 30 minutes, and then red/green fluorescent intensity was determined using a FACSverse (BD Biosciences) flow cytometer. MOMP was determined using a mitochondrial permeability transition pore (MPTP) assay kit (BioVision) according to the manufacturer's instructions. In brief, NRCMs were resuspended in prewarmed MPTP Wash Buffer at a final concentration of  $1 \times 10^6$  cells  $\text{mL}^{-1}$  and then stained with MPTP Staining Dye for 15 minutes at 37°C at the presence of cobalt chloride. After washing, the cells were resuspended in MPTP Wash Buffer and analyzed using a FACSverse flow cytometer. Data analysis was performed using FlowJo software (TreeStar).

#### MYOCARDIAL MITOCHONDRIAL OXIDATIVE DAMAGE MEASUREMENT.

Myocardial mitochondria were isolated using a Tissue or Cell Mitochondria Isolation Kit (Beyotime) following the manufacturer's instructions. To determine mitochondrial lipid peroxidation, mitochondrial malondialdehyde concentration was measured using a thiobarbituric acid reactive substances assay kit (Cayman Chemical). Briefly, thiobarbituric acid was reacted with malondialdehyde in the samples at 100°C, followed by the measurement using a microplate reader. Mitochondrial 8-hydroxy-2-deoxyguanosine was measured using an 8-hydroxy-2-deoxyguanosine enzyme-linked immunosorbent assay kit following the manufacturer's instructions.

#### RNA EXTRACTION AND QUANTITATIVE POLYMERASE CHAIN REACTION.

Total RNA was isolated using RNAiso Plus (TaKaRa) and was reversely transcribed using a PrimerScript RT Master Mix (TaKaRa) according to the manufacturer's instructions. The messenger RNA expression levels of indicated genes were examined by quantitative polymerase chain reaction using a SYBR Green qPCR Master Mix (MedChem Express) on a CFX96TM Real-Time system (Bio-Rad). Data were normalized relative to

**FIGURE 1** Mitochondrial Oxidative Damage Is Early and Prominent in Cardiomyocytes in a CKD Milieu

GAPDH. For analysis of mtDNA copy number, nuclear DNA and mtDNA were extracted using a DNeasy Blood and Tissue kit (Qiagen), and mtDNA copy numbers were quantified by quantitative polymerase chain reaction using a CFX96 Real-Time system. The level of ND1 (mtDNA) was normalized to the level of B2M (nuclear DNA). Primer sequences are listed in [Supplemental Table 1](#).

**RNA SEQUENCING.** Total RNA was extracted, and RNA concentration and integrity were determined by an Agilent 2100 Bioanalyzer using an Agilent RNA 2100 Nano Kit (all Agilent Technologies). Library construction and RNA sequencing were performed at the Beijing Genomics Institute. The prepared library was sequenced with DNA Nanoballs Sequencing platform. All RNA sequencing raw reads were first filtered using SOAPnuke version 1.5.2 to obtain clean reads.<sup>19</sup> After sequence alignment, gene expression was quantified using RSEM version 1.2.8,<sup>20</sup> and differential gene expression evaluation was analyzed by DESeq2 using a fold change  $\geq 2.00$  and adjusted *P* value  $< 0.05$ . Gene set enrichment analysis (Broad Institute, UC San Diego) was performed on the basis of Molecular Signatures Database version 6.0) and Gene Expression Omnibus (National Center for Biotechnology Information).

**RNA INTERFERENCE.** NRCMs were separately transfected with small interfering RNAs (siRNAs) including siODC1, sip65, sicGAS, siSTING, and siMAVS (all GenePharma) using HiPerFect transfection reagent (Qiagen) according to the manufacturer's instructions. Briefly, siRNAs were dissolved by ribonuclease-free H<sub>2</sub>O and stored at a concentration of 20  $\mu\text{M}$ . To knock down targeted genes, 2  $\mu\text{L}$  siRNA and 3  $\mu\text{L}$  HiPerFect transfection reagent were diluted in 100  $\mu\text{L}$  serum-free M199 medium (Sigma-Aldrich) and incubated for 10 minutes at room temperature to allow the formation of

transfection complexes. Then, the complexes were added dropwise onto the cells and the plate was gently swirled to ensure uniform distribution of the transfection complexes, followed by incubation for 48 hours. The final concentration of siRNAs was 20 nM. Finally, the transfected cells were used for the subsequent experiments. The siRNA sequences are listed in [Supplemental Table 2](#).

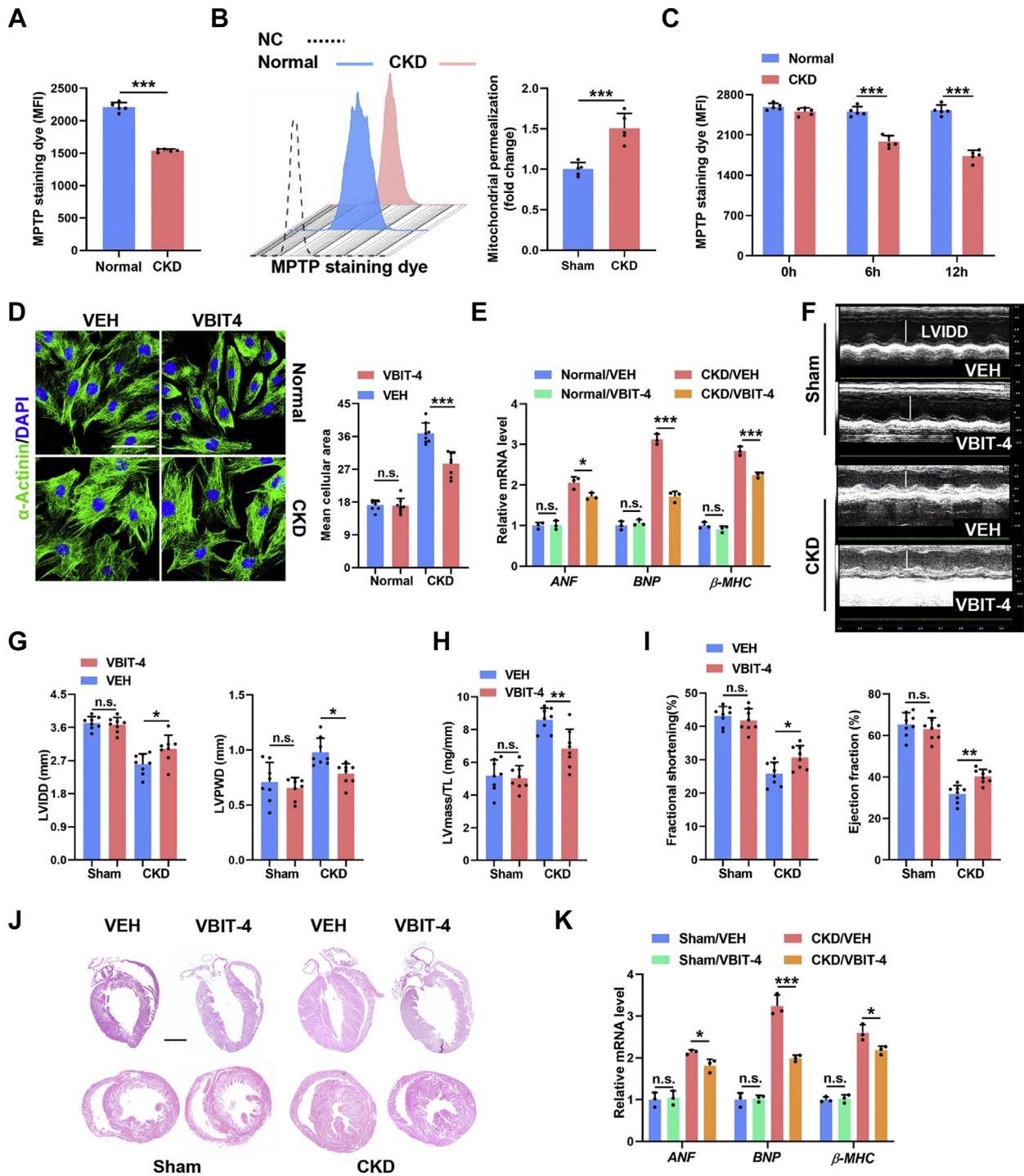
**FLAG-cGAS CLONING AND CHROMATIN IMMUNOPRECIPITATIONS.** Chromatin immunoprecipitation was performed using a SimpleChIP Enzymatic Chromatin IP Kit (Cell Signaling Technology) according to the manufacturer's instructions. Briefly, myocardia or NRCMs were fixed with formaldehyde (Cell Signaling Technology) to crosslink proteins to DNA. Then, the chromatin was fragmented using sonication and immunoprecipitated with antibody specific to p65 (catalog #8242S, Cell Signaling Technology). Subsequently, the protein-DNA crosslinks were reversed, and genomic DNA was purified. Finally, the enriched DNA fragments were detected by polymerase chain reaction.

3 $\times$ Flag-tagged rat cGAS was subcloned into a pCDH-CMV-MCS-EF1-GFP+Puro lentiviral vector (Genecreate). The lentivirus was produced by Genecreate using transient transfection of 293T cells with a 3-vector packaging system. The virus supernatant was collected after transfection for 48 hours and concentrated by centrifugation at 25,000 rpm for 2 hours at 4°C. The virus pellet was resuspended, subpackaged, and stored at  $-80^{\circ}\text{C}$ . A total of  $2 \times 10^5$  NRCMs were transduced of 25  $\mu\text{L}$  lentivirus ( $2.4 \times 10^8$  TU/mL, multiplicity of infection = 30) for 24 hours. Then, the transduced NRCMs were incubated with normal or CKD serum for another 48 hours. Subsequently, chromatin immunoprecipitation was performed as described previously using an anti-FLAG M2 antibody (Sigma-Aldrich). The DNA

**FIGURE 1 Continued**

(A) Kyoto Encyclopedia of Genes and Genomes enrichment analysis and Gene Ontology enrichment analysis show top down-regulated pathways in myocardia from chronic kidney disease (CKD) mice. (B) Representative transmission electron microscopic images of mitochondria in primary neonatal rat cardiomyocytes (NRCMs) incubated with normal or CKD serum. The **box** indicates the region magnified in the **bottom panel**. The **arrow** indicates the swollen and vacuolated mitochondria. Scale bars, 2  $\mu\text{m}$  in the **top panel** and 0.5  $\mu\text{m}$  in the **bottom panel**. (C) Quantification of complex IV and mitochondrial membrane potential (MMP) in the myocardia from sham and CKD mice. (D) Seahorse analysis of oxygen consumption rate (OCR) and basal and maximum respiration levels in NRCMs incubated with normal or CKD serum. (E) Representative flow cytometry analysis and quantification of mitochondrial membrane potential in NRCMs incubated with normal or CKD serum. (F) Representative images of dihydroethidium (DHE) staining in myocardia from sham and CKD mice. Scale bar, 40  $\mu\text{m}$ . (G) Quantification of 2',7'-dichlorodihydrofluorescein diacetate (DCFH-DA) in NRCMs after incubation with normal or CKD serum. (H) Contents of malondialdehyde (MDA) and 8-hydroxy-2-deoxyguanosine (8-OHdG) in myocardia from sham and CKD mice. (I) Contents of MDA and 8-OHdG in NRCMs after incubation with normal or CKD serum. (J) Representative images of DCFH-DA staining in NRCMs after incubation with normal or CKD serum for 0, 6, and 12 hours. (K) Contents of DCFH-DA, MMP, atrial natriuretic factor (ANF), brain natriuretic peptide (BNP), and myosin heavy chain ( $\beta$ -MHC) in NRCMs after incubation with normal or CKD serum for 0, 6, and 12 hours. Data are represented as mean  $\pm$  SD and were analyzed using 2-tailed Student's *t*-tests.  $n = 3$  biologically independent experiments.  $***P < 0.001$ . JC-1 = 5,5',6,6'-tetrachloro-1,1',3,3'-tetraethylbenzimidazolcarbocyanine iodide; TCA = tricarboxylic acid.

**FIGURE 2** VDAC1-Mediated Mitochondrial Outer Membrane Permeabilization Commits Cardiomyocytes to Undergo Hypertrophy in a CKD Milieu



Continued on the next page

abundance of whole-cell extracts served as normalization control for the immunoprecipitated DNA abundance. The primer sequences and antibodies used are listed in [Supplemental Tables 3 and 4](#).

#### NONINVASIVE BLOOD PRESSURE MEASUREMENTS.

Systolic blood pressures were noninvasively measured in conscious animals using the tail-cuff method<sup>21</sup> (ML125, PowerLab, AD Instruments). Briefly, mice were placed in a cylindrical holder on a temperature-controlled platform (kept at 37°C), and recordings were performed in steady-state conditions. Blood pressure values were averaged from 3 consecutive measurements.

**WESTERN BLOT.** Total protein was extracted by RIPA lysis buffer with cOmplete EDTA-free Protease Inhibitor Cocktail and PhosSTOP Phosphatase Inhibitor Cocktail (all Roche Molecular Systems) for 30 minutes at 4°C. To isolate nuclear proteins, the Nuclei Pure Prep kit (NUC-201, Sigma-Aldrich) was used according to the manufacturer's instructions. The protein concentrations were determined by a BCA protein assay kit (Thermo Fisher Scientific). Protein expression levels were determined using anti-p65 (catalog #8242S), anti-histone H3 (catalog #4499S), anti-p-IKB $\alpha$  (catalog #2859), anti-IKB $\alpha$  (catalog #4814), anti-STING (catalog #13647s), anti-TBK1(catalog #38066s), anti-p-TBK1 (catalog #5483s), anti-GAPDH (catalog #5174s) (all Cell Signaling Technology), anti-cGAS (catalog #sc-515777), and anti-ODC1 (catalog #sc-390366) (both Santa Cruz Biotechnology) antibodies at 4°C overnight. Then, the membranes were incubated with secondary antibodies (catalog #205718 or catalog #205719, Abcam) for 1 hour at room temperature and scanned using a Bio-Rad ChemiDoc MP imager. Band intensity was quantified using Image Lab version 5.1 (Bio-Rad) and normalized relative to GAPDH, and the intensity for phosphorylated proteins was normalized relative to appropriate total protein. The intensity for the nuclear proteins was normalized

relative to histone H3. Detailed information of antibodies is listed in [Supplemental Table 4](#).

**TRANSMISSION ELECTRON MICROSCOPY.** NRCMs were fixed in 2.5% glutaraldehyde and sent to the Biomedical Analysis Center of Army Medical University (Third Military Medical University) for standard transmission electron microscopic ultrastructural analysis. Sections were photographed using a JEM-1400 transmission electron microscope (JEOL).

**HISTOLOGIC EVALUATION.** Isolated hearts were fixed using 4% paraformaldehyde, dehydrated, and embedded in paraffin. Hearts were sectioned serially into 4- $\mu$ m-thick slices and stained with hematoxylin and eosin. The sections were photographed using an Olympus Optical microscope (Olympus Optical).

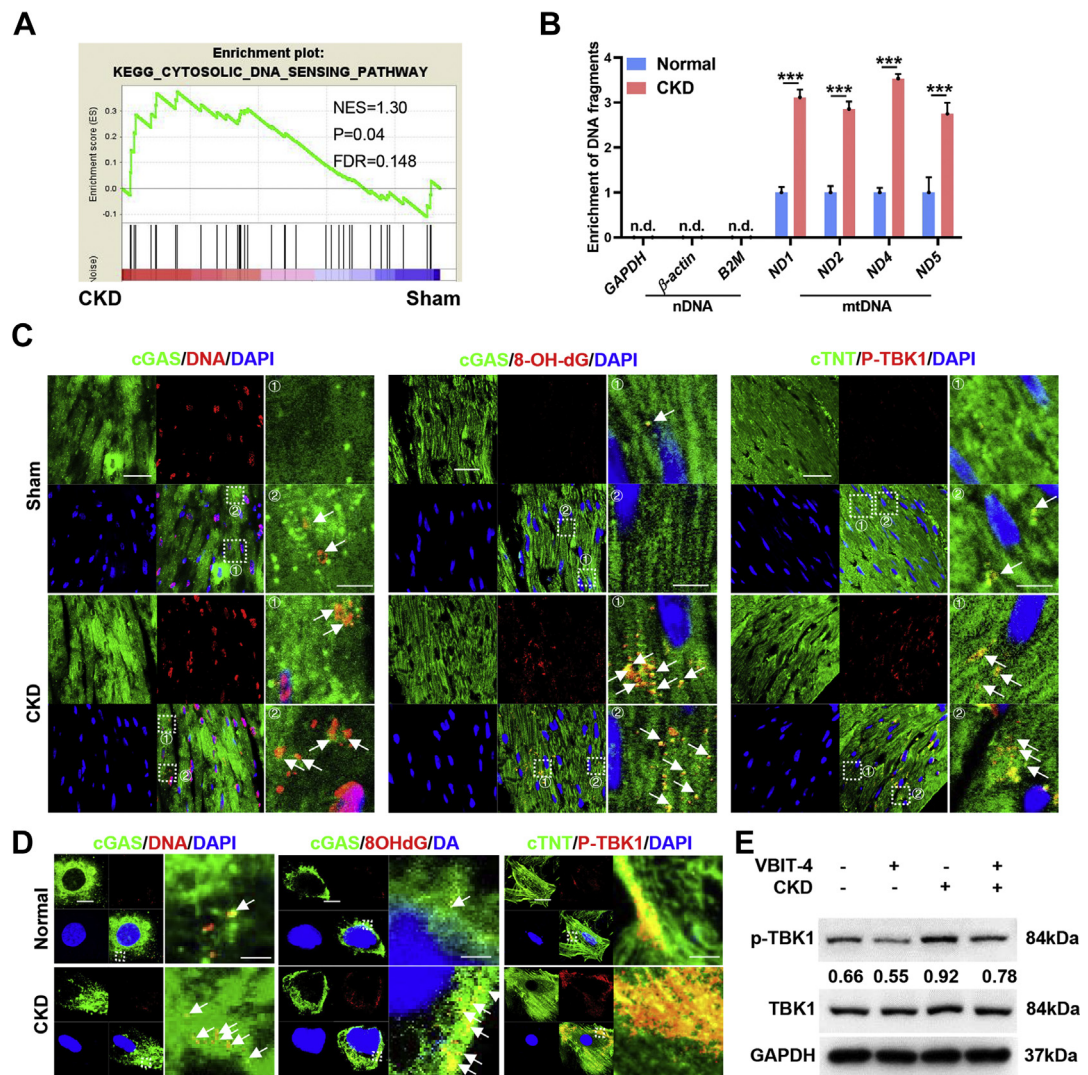
**IMMUNOFLOUORESCENCE.** Paraffin sections were obtained as described earlier. Frozen samples were sliced into 4- $\mu$ m thickness. Frozen sections and cells were fixed with 4% paraformaldehyde, followed by permeabilization and blocking using 0.25% Triton X-100 and 5% goat serum (all Santa Cruz Biotechnology), respectively. Sections and cells were stained for anti- $\alpha$ -actinin (catalog #69758s), anti-p65 (catalog #8242s), anti-p-TBK1 (catalog #5483s), anti-cGAS (catalog #sc-515777) (all Cell Signaling Technology), anti-cTNT (catalog #bs-10648r, Beijing Biosynthesis Biotechnology), anti-DNA (catalog #CBL186, Sigma-Aldrich), and anti-8-OHdG (catalog #ab48508, Abcam) antibodies at 4°C overnight. Primary antibodies were labeled with fluorescent dye-conjugated secondary antibodies (catalog #A-11001, #A-11003, #A-11008, and #A-11010, all Thermo Fisher Scientific) and 4',6-diamidino-2-phenylindole and photographed using a confocal laser-scanning microscope (LSM780, Carl Zeiss). Detailed information of antibodies is listed in [Supplemental Table 4](#).

#### HIGH-PERFORMANCE LIQUID CHROMATOGRAPHIC ANALYSIS OF POLYAMINES.

Myocardia or NRCMs were homogenized in RIPA lysis buffer with 1  $\mu$ L internal standard (hexamethylenediamine, 10  $\mu$ mol mL<sup>-1</sup>),

#### FIGURE 2 Continued

(A) Quantification of mitochondrial permeabilization in NRCMs incubated with normal or CKD serum. (B) Representative flow cytometry plots and quantification of mitochondrial permeability transition pore (MPTP) permeability in NRCMs incubated with normal or CKD serum for 48 hours. (C) Quantification of MPTP in NRCMs incubated with normal or CKD serum for 0, 6, and 12 hours. (D) Representative images of  $\alpha$ -actinin staining in normal and CKD serum-incubated NRCMs with or without VBIT-4 treatment. Scale bars, 20  $\mu$ m. (E) Relative messenger RNA (mRNA) levels of ANF, BNP, and  $\beta$ -MHC in normal and CKD serum-incubated NRCMs with or without VBIT-4 treatment. (F to I) Echocardiographic examination of left ventricular internal diameter at diastole (LVIDD), left ventricular posterior wall thickness at end-diastole (LVPWD), ejection fraction, fractional shortening, and left ventricular (LV) mass in each group. LV mass/tibial length (TL) ratio was calculated. (J) Representative hematoxylin and eosin staining of sagittal and midchamber sections of the hearts. Scale bar, 200  $\mu$ m. (K) Relative mRNA levels of ANF, BNP, and  $\beta$ -MHC in myocardia from sham and CKD mice with or without VBIT-4 supplementation. Data are represented as mean  $\pm$  SD and were analyzed using 2-tailed Student's *t*-tests (A to C) or 1-way analysis of variance (D, E, G to I, K). *n* = 3 biologically independent experiments. \**P* < 0.05, \*\**P* < 0.01, and \*\*\**P* < 0.001. n.s. = not significant; VEH = vehicle; other abbreviations as in [Figure 1](#).

**FIGURE 3** Mitochondrial Outer Membrane Permeabilization-Mediated mtDNA Release Stimulates the cGAS-STING Pathway in Cardiomyocytes in a CKD Milieu

(A) Gene set enrichment analysis of gene sets associated with cytosolic DNA sensing pathway in the myocardia. (B) Relative enrichment of DNA fragments in NRCMs incubated with normal or CKD serum. (C) Representative images of cGAS and DNA (left), cGAS and 8-OHdG (middle), or cardiac troponin T (cTNT) and p-TBK1 (right) colocalization in the myocardia. The region marked by the box is magnified in the right panel. Colocalization of cGAS with DNA (left), colocalization of cGAS with 8-OHdG (middle), and colocalization of cTNT with p-TBK1 (right) are marked by the white arrow. Scale bar, 20  $\mu$ m in the left panels and 4  $\mu$ m in the right panels. (D) Representative images of cGAS and DNA (left), cGAS and 8-OHdG (middle), or cTNT and p-TBK1 (right) colocalization in NRCMs incubated with normal or CKD serum. The region marked by the box is magnified in the right panel. Colocalization of cGAS with DNA (left) and colocalization of cGAS with 8-OHdG (middle) with p-TBK1 (right) are marked by the white arrow. Scale bar, 20  $\mu$ m in left panel and 4  $\mu$ m in the right panel. (E) Representative western blot analysis of p-TBK1 in the myocardia from sham or CKD mice with or without VBIT-4 treatment. Data represent mean  $\pm$  SD and were analyzed using 2-tailed Student's *t*-test (B) or 1-way analysis of variance (E).  $n = 3$  biologically independent experiments. \*\* $P < 0.01$  and \*\*\* $P < 0.001$ . DAPI = 4',6-diamidino-2-phenylindole; FDR = false discovery rate; mtDNA = mitochondrial DNA; n.d., not determined; nDNA = nuclear DNA; NES = normalized enrichment score; other abbreviations as in Figure 1.

and protein concentrations were measured using a BCA protein assay kit. Then, 1,000  $\mu$ L perchloric acid (5%) was added to precipitate proteins. After incubating for 30 minutes, the homogenate was

centrifuged for 10 minutes at 14,000g at 4°C, and supernatant was taken for derivatization reaction. The supernatant was mixed with 1,000  $\mu$ L NaOH (2 mM) and 8  $\mu$ L benzoyl chloride for

20 minutes. Subsequently, 2 mL chloroform and equivalent 0.9% normal saline were added and vortexed for 1 minutes. The liquid was further separated after centrifugation for 10 minutes at 3,000g. The underlayer solution that contained polyamines was dried by nitrogen and resuspended with methanol before incubating in 50°C water for 8 hours. Subsequently, 2 mL chloroform and 200  $\mu$ L NaOH were added for further purification. The polyamine derivatives were detected using C18 high-performance liquid chromatography columns (250  $\times$  4.6 mm, 5  $\mu$ M) with a Waters e2489 UV/Visible detector. The excitation and emission wavelengths of the detector were set at 229 nm. The solvent flow was 1 ml min<sup>-1</sup> (5% methanol:95% methanol, 45:55 vol/vol). The runtime was 50 minutes for each sample. Column temperature was maintained at 37°C. The injection volume was 10  $\mu$ L per sample.

**STATISTICAL ANALYSIS.** All data were analyzed using Prism version 8.0 (GraphPad Software). One-way analysis of variance for 3 or more groups followed by Tukey's post hoc test for multiple pairwise comparisons or Student's *t*-test for 2 groups was used to compare means. The number of independent experiments is identified in the figure legends as *n*. All data are expressed as mean  $\pm$  SD. A 2-sided *P* value <0.05 was considered to indicate statistical significance.

## RESULTS

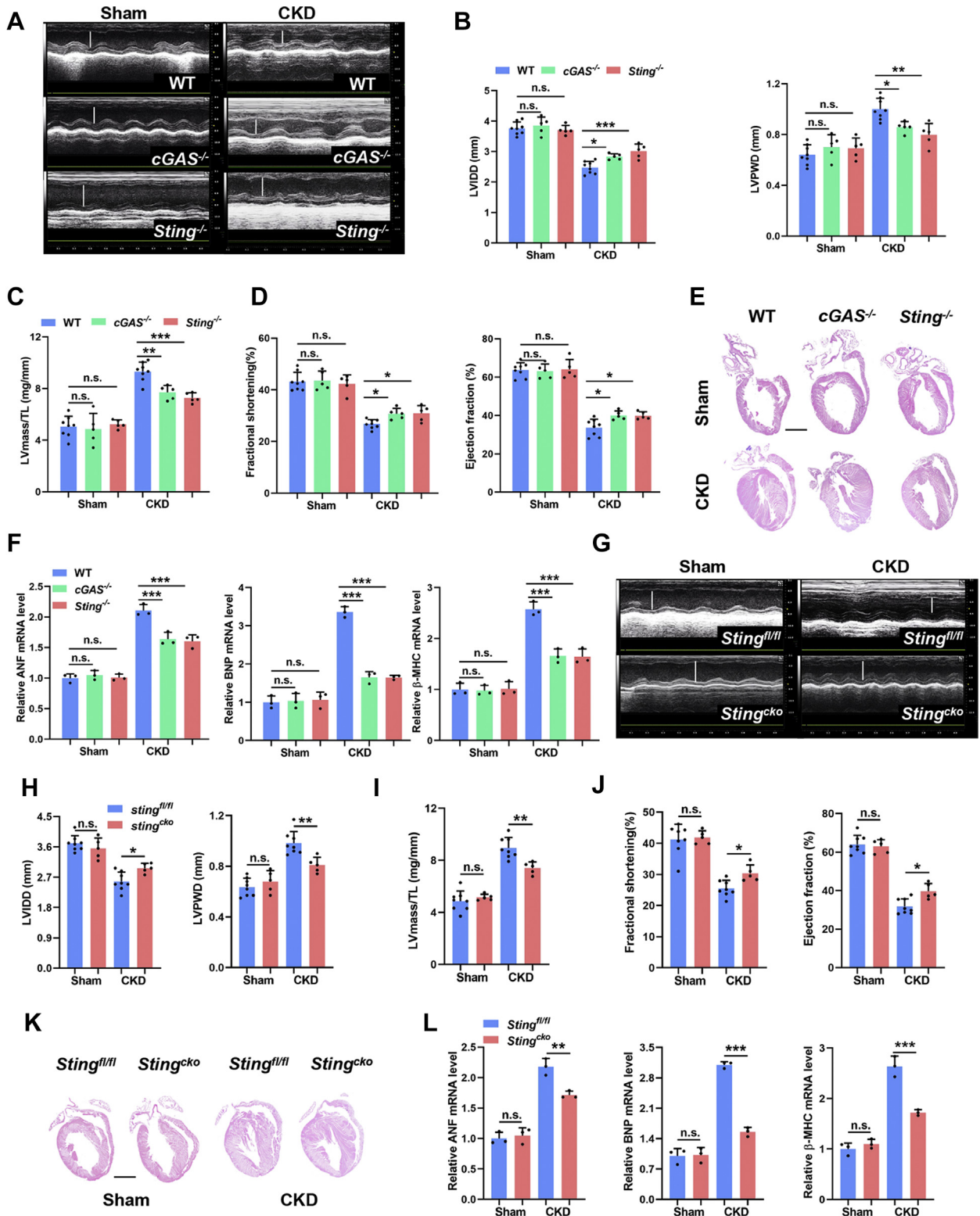
**MITOCHONDRIAL OXIDATIVE DAMAGE IS EARLY AND PROMINENT IN CARDIOMYOCYTES IN A CKD MILIEU.** Initially, RNA sequencing-based gene expression landscapes of myocardia from sham-operated and CKD mice were obtained (Supplemental Figure 1A). RNA sequencing revealed significant down-regulation of cardiac muscle contraction-related genes (Figure 1A) and up-regulation of ventricular hypertrophy-related genes (Supplemental Figure 1B) in the myocardia of CKD mice, thus confirming pathologic cardiac hypertrophy in CKD mice at the transcription level. Consistently, significantly increased expression levels of cardiac hypertrophic markers including atrial natriuretic factor, brain natriuretic peptide, and myosin heavy chain were verified in cardiomyocytes in a CKD milieu (Supplemental Figure 1C). Notably, we found that down-regulation of mitochondrial genes was most prominent in the myocardia of CKD mice (Figure 1A). Meanwhile, mitochondrial swelling and vacuolation were frequently observed in cardiomyocytes in a CKD milieu (Figure 1B), accompanied by dramatically declined mitochondrial respiratory function and mitochondrial membrane potential both in vivo

(Figure 1C) and in vitro (Figures 1D and 1E). These results indicate that mitochondria are damaged in cardiomyocytes in a CKD milieu, and this phenomenon is prominent.

Mitochondria are sensitive to oxidative stress, which is the most outstanding characteristic of the CKD milieu.<sup>22</sup> Accordingly, ROS overproduction was observed in cardiomyocytes in a CKD milieu (Figures 1F and 1G). Besides, significantly increased mitochondrial lipid peroxidation and mtDNA oxidation in the myocardia and cardiomyocytes were also detected in vivo and in vitro (Figures 1H and 1I). Surprisingly, ROS production was immediately increased in cardiomyocytes in a CKD milieu in vitro (Figure 1J), preceding the appearance of mitochondrial damage (Figure 1K). On the contrary, scavenging ROS by *N*-acetylcysteine significantly abrogated CKD-induced mitochondrial oxidative damage in cardiomyocytes (Supplemental Figures 1D to 1G). Moreover, mitochondrial damage occurred before the appearance of noticeable cardiomyocyte hypertrophy in a CKD milieu (Figure 1K). Given that *N*-acetylcysteine also significantly alleviated CKD-induced cardiomyocyte hypertrophy (Supplemental Figure 1H), mitochondrial oxidative damage might be involved in the initiation of CKD-induced cardiomyocyte hypertrophy.

**VDAC1-MEDIATED MOMP COMMITS CARDIOMYOCYTES TO UNDERGO HYPERTROPHY IN A CKD MILIEU.** Mitochondrial damage will alert the cell through MOMP, which releases mitochondrial factors including cytochrome *c* as well as mtDNA and double-stranded RNA to stimulate the apoptotic cascade or innate immune signaling respectively, hence inducing cell-intrinsic adaptive responses.<sup>23</sup> Indeed, immediately and significantly increased mitochondrial permeability was detected in cardiomyocytes in a CKD milieu both in vivo and in vitro (Figures 2A to 2C). MOMP is mediated mainly by BAX/BAK oligomers or VDAC oligomers in the mitochondrial outer membrane.<sup>23,24</sup> On the basis of RNA sequencing, we found that VDAC1 was expressed predominantly in the myocardia (Supplemental Figure 2A). To interrogate whether MOMP initiated CKD-induced cardiomyocyte hypertrophy, BAX/BAK- or VDAC1-mediated MOMP was inhibited by BAI1 or VBIT-4, respectively. Interestingly, only VBIT-4 treatment remarkably abolished CKD-induced cardiomyocyte hypertrophy in vitro (Figures 2D and 2E, Supplemental Figure 2B), similar to the effects of *N*-acetylcysteine treatment. Similarly, VBIT-4 treatment significantly prevented cardiac hypertrophy in CKD mice (Figures 2J and 2K), which is characterized by decreased LV internal diameter at diastole and increased LV posterior wall

**FIGURE 4** Activation of the Myocardial cGAS-STING Pathway Drives Cardiac Hypertrophy



thickness at end-diastole (Figures 2F and 2G), as well as elevated LV mass/tibial length ratio (Figure 2H), accompanied by significantly improved ventricular contractility and cardiac output (Figure 2I). Notably, apoptotic cell death was almost unaffected in cardiomyocytes in a CKD milieu in vitro (Supplemental Figure 2C), consistent with BAX/BAK-mediated MOMP occurring mainly in apoptosis.<sup>21</sup> These findings indicate that VDAC1-mediated MOMP is crucial for the initiation of CKD-induced cardiac hypertrophic response.

**MOMP-MEDIATED mtDNA RELEASE STIMULATES THE cGAS-STING PATHWAY IN CARDIOMYOCYTES IN A CKD MILIEU.** Subsequently, we found that cytosolic DNA sensing rather than double-stranded RNA sensing was significantly activated in cardiomyocytes in a CKD milieu (Figures 3A and 3B, Supplemental Figure 3A). cGAS is the primary DNA sensor in mammals, stimulation of which will activate the adaptor protein STING.<sup>25</sup> Accordingly, colocalization of mtDNA, especially oxidized mtDNA, with cGAS was dramatically increased in cardiomyocytes in a CKD milieu both in vivo and in vitro, accompanied by significant activation of TANK-binding kinase 1 (TBK1), a key kinase downstream of the cGAS-STING pathway (Figures 3C and 3D, Supplemental Figures 3B and 3C). Meanwhile, VBIT-4 treatment significantly suppressed CKD-induced activation of the cGAS-STING pathway in cardiomyocytes (Figure 3E). Therefore, the cGAS-STING pathway is distinctively stimulated by MOMP-mediated mtDNA release in a CKD milieu.

**ACTIVATION OF THE MYOCARDIAL cGAS-STING PATHWAY DRIVES CARDIAC HYPERTROPHY IN CKD.** Next, we investigated whether activation of the cGAS-STING pathway contributed to the initiation of CKD-induced cardiac hypertrophy. It was found that defect of the cGAS-STING pathway but not double-stranded RNA sensing melanoma differentiation-associated gene 5-mitochondria antiviral signaling protein (MDA5-MAVS) pathway evidently attenuated CKD-induced cardiomyocyte hypertrophy (Figures 4A to 4F, Supplemental Figures 3D to 3H). As the cGAS-STING pathway is highly active in immune cells, which are also implicated in the pathogenesis of

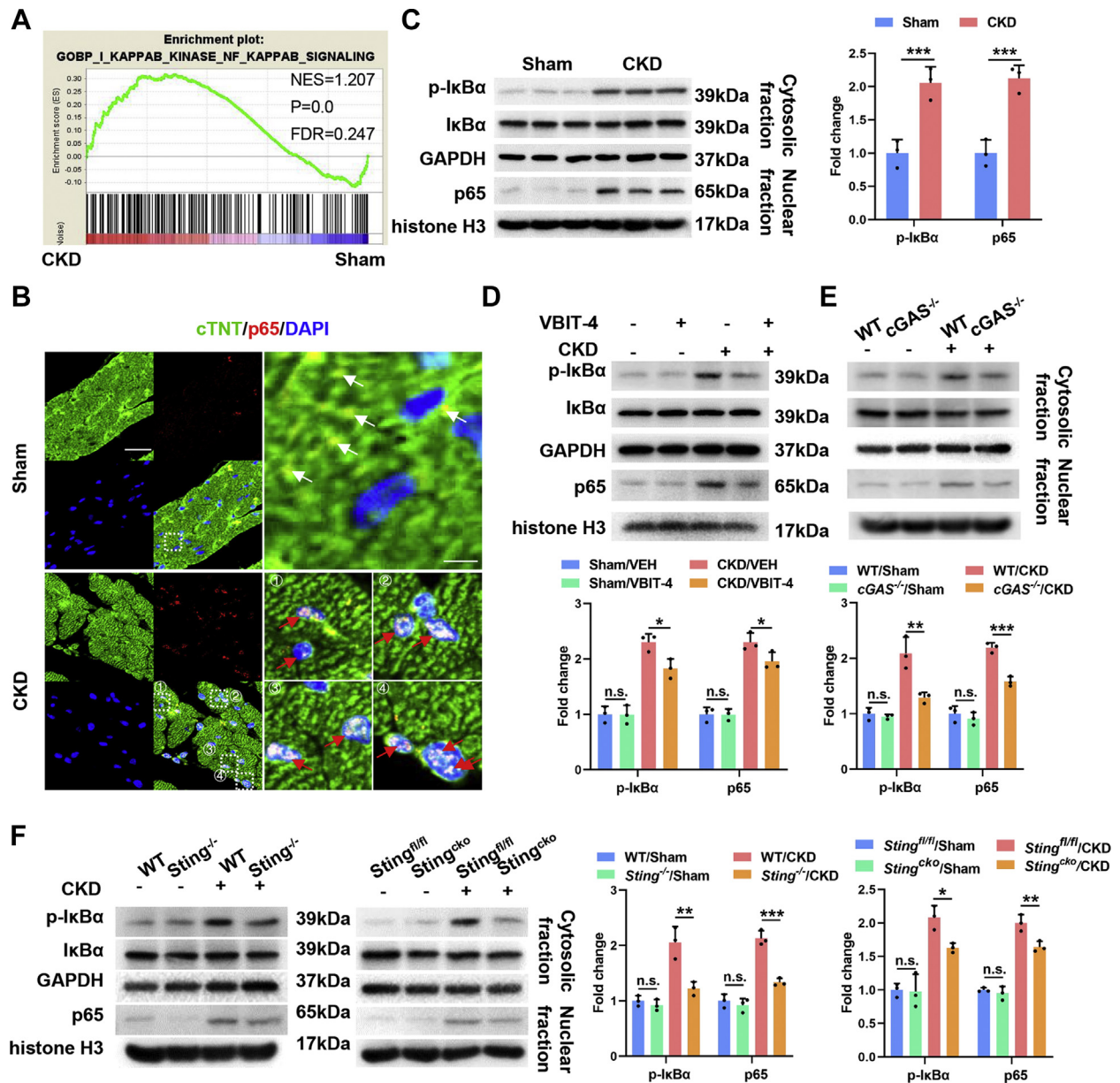
cardiac hypertrophy,<sup>26</sup> we further verified the distinct role of the myocardial cGAS-STING pathway using a cardiomyocyte-specific STING-deficient (*Sting<sup>ckc</sup>*) mice. Similarly, myocardial ablation of STING also significantly alleviated cardiac hypertrophy in CKD mice (Figures 4G to 4L), without affecting the pressure overload (Supplemental Figure 3J). Altogether, these results demonstrate that the activation of myocardial cGAS-STING pathway promotes the initiation of CKD-induced cardiac hypertrophy.

**NFκB ACTS DOWNSTREAM OF THE cGAS-STING PATHWAY TO DRIVE CARDIAC HYPERTROPHIC PROGRAM IN A CKD MILIEU.** Interferon regulatory factor 3 (IRF3) and NFκB/p65 are the main downstream effectors of the cGAS-STING pathway.<sup>25</sup> We found that myocardial NFκB signaling was significantly activated in a CKD milieu, manifested by significantly increased nuclear translocation of p65 and phosphorylation of its inhibitory IκB protein (Figures 5A to 5C, Supplemental Figures 4A and 4B). Unexpectedly, myocardial IRF3 activity was comparable in a CKD milieu with that under basal condition (Supplemental Figures 4C and 4D). Meanwhile, both inhibition of MOMP and defect of the cGAS-STING pathway significantly inhibited myocardial NFκB activation in a CKD milieu (Figures 5D to 5F, Supplemental Figure 4E). In addition, pharmacologic inhibition of p65 by a clinically tolerated inhibitor, ammonium pyrrolidinedithiocarbamate, dramatically alleviated CKD-induced cardiac hypertrophy (Supplemental Figures 4F and 4G). Similar results were observed in vitro when myocardial p65 was knocked down using siRNA (Supplemental Figures 4H to 4J). Given that NFκB transcriptionally drives the cardiac hypertrophic program,<sup>27-29</sup> these results indicate a key role of myocardial NFκB signaling that acts downstream of the cGAS-STING pathway in driving cardiac hypertrophic program in a CKD milieu.

**ODC1-PUT METABOLIC FLUX IS INDISPENSABLE FOR STING-NFκB PATHWAY-DRIVEN CARDIAC HYPERTROPHIC PROGRAM IN A CKD MILIEU.** RNA sequencing also revealed activated polyamine metabolism in the myocardia of CKD mice, manifested by up-regulated expression of polyamine

**FIGURE 4 Continued**

(A to D) Echocardiographic examination of LVIDD, LVPWD, ejection fraction, fractional shortening, and LV mass in each group. LV mass/TL ratio was calculated. (E) Representative hematoxylin and eosin staining of sagittal sections of the hearts. Scale bar, 200 μm. (F) Relative mRNA levels of ANF, BNP, and β-MHC in the myocardia from *cGAS<sup>-/-</sup>* and *Sting<sup>-/-</sup>* mice with or without CKD. (G to J) Echocardiographic examination of LVIDD, LVPWD, ejection fraction, fractional shortening, and LV mass in each group. LV mass/TL ratio was calculated. (K) Representative hematoxylin and eosin staining of sagittal sections of the hearts. Scale bar, 200 μm. (L) Relative mRNA levels of ANF, BNP, and β-MHC in myocardia in each group. Data represent mean ± SD and were analyzed using 1-way analysis of variance. n = 3 biologically independent experiments. \*P < 0.05, \*\*P < 0.01, and \*\*\*P < 0.001. Abbreviations as in Figures 1 and 2.

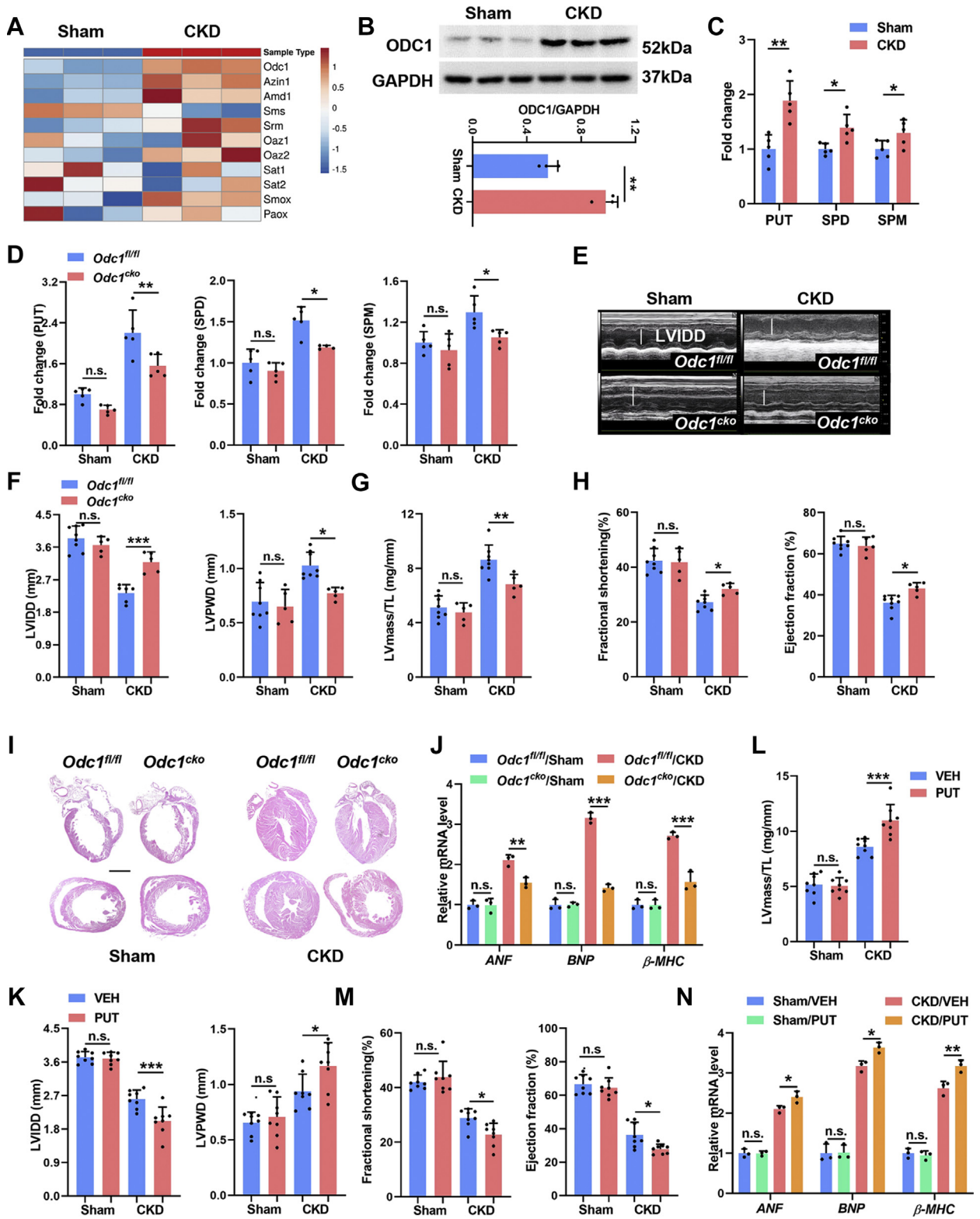
**FIGURE 5** NF $\kappa$ B Acts Downstream of the cGAS-STING Pathway to Drive Cardiac Hypertrophic Program in a CKD Milieu

(A) Gene set enrichment analysis of Ik $\beta$  kinase NF $\kappa$ B signaling in the myocardia. (B) Representative images of p65 and cTNT staining in the myocardia. The region marked by the box is magnified in the right panel. Cytoplasmic p65 is marked by white arrows, and nuclear p65 is marked by red arrows. Scale bar, 20  $\mu$ m in the left panels and 4  $\mu$ m in the right panels. (C) Representative western blot (WB) analysis of p-Ik $\beta$  and p65 in the myocardia. (D) Representative WB analysis of p-Ik $\beta$  and p65 in the myocardia from sham and CKD mice with or without VBIT-4 treatment. (E) Representative WB analysis of p-Ik $\beta$  and p65 in the myocardia from sham and CKD mice in each group. (F) Representative WB analysis of p-Ik $\beta$  and p65 in the myocardia from sham and CKD mice in each group. Data represent mean  $\pm$  SD and were analyzed using 2-tailed Student's *t*-test (C) or 1-way analysis of variance (D to F). *n* = 3 biologically independent experiments. \**P* < 0.05, \*\**P* < 0.01, and \*\*\**P* < 0.001. WT = wild-type; other abbreviations as in Figures 1 to 3.

biosynthetic enzymes, especially ODC1, and comparable expression of polyamine catabolic enzymes (Figure 6A). Meanwhile, ODC1 up-regulation was also verified at the protein level in the myocardia of CKD

mice (Figure 6B). Accordingly, higher levels of polyamines, especially PUT, were detected in the cardiomyocytes in a CKD milieu both in vivo and in vitro (Figure 6C, Supplemental Figure 5A). ODC1 is

**FIGURE 6** Activation of Myocardial ODC1-PUT Metabolic Flux Is Required for CKD-Induced Cardiac Hypertrophy



the unique rate-limiting enzyme of polyamine metabolism that catalyzes PUT biosynthesis.<sup>14</sup> Then, we specifically deleted or knocked down ODC1 in cardiomyocytes using *Myh6-Cre<sup>+</sup>Odc1<sup>fllox/fllox</sup>* (*Odc1<sup>cko</sup>*) mice or RNA interference, respectively, and found that myocardial ODC1 deficiency dramatically counteracted CKD-induced polyamine accumulation in cardiomyocytes (Figure 6D, Supplemental Figure 5C). Notably, myocardial ODC1 deficiency also dramatically counteracted CKD-induced cardiac hypertrophy both in vivo (Figures 6E to 6J) and in vitro (Supplemental Figures 5D and 5E). On the contrary, although PUT supplementation alone induced negligible effects, it significantly aggravated CKD-induced cardiac hypertrophy both in vivo (Figures 6K to 6N) and in vitro (Supplemental Figures 5F and 5G). These results demonstrate that the activation of myocardial ODC1-PUT metabolic flux is not an independent pathogenetic factor but is indispensable for the initiation of CKD-induced cardiac hypertrophy.

Further study also revealed that blockade of the STING-NFκB pathway significantly blunted CKD-induced ODC1 up-regulation and PUT accumulation in cardiomyocytes both in vivo (Supplemental Figures 6A to 6C) and in vitro (Figures 7A to 7C). The positive correlation between NFκB activity and ODC1 expression in cardiomyocytes suggested that ODC1 might be a transcriptional target of NFκB. Indeed, bioinformatics analysis found several potential NFκB-binding sites in the promoter regions of human, mouse, and rat *Odc1* gene (Table 1). Then, chromatin immunoprecipitation assay demonstrated that NFκB could bind directly to the *Odc1* promoter, whereas CKD remarkably enhanced this binding (Figure 7D). Therefore, NFκB may conservatively regulate ODC1-PUT metabolic flux in cardiomyocytes at the transcription level. More interestingly, PUT supplementation could offset the protective effects of myocardial ODC1 deficiency on CKD-induced cardiomyocyte hypertrophy but failed to offset those of

STING-NFκB pathway inhibition (Figures 7E to 7H). Altogether, these data indicate that ODC1-PUT metabolic flux is required for STING-NFκB pathway-driven cardiac hypertrophic program in a CKD milieu.

**PHARMACOLOGIC INHIBITION OF THE MITOCHONDRIA-STING-POLYAMINE AXIS PREVENTS CARDIAC HYPERTROPHY IN CKD.** In the foregoing results, we have proved the therapeutic potential of targeting MOMP by VBIT-4 and targeting NFκB by ammonium pyrrolidinedithiocarbamate. To strengthen the translational potential of our findings, we further tested the effect of a STING inhibitor, C-176,<sup>30</sup> on CKD-induced cardiac hypertrophy. As did the effects of myocardial STING ablation, C-176 treatment also significantly blunted the accumulation of polyamines in the myocardia and finally alleviated the cardiac hypertrophy in CKD mice (Figures 8A to 8G). Furthermore, oral administration of a clinically available ODC1 inhibitor, difluoromethylornithine, also significantly prevented cardiac hypertrophy in CKD mice (Figures 8H to 8M), similar to the effects of myocardial ODC1 ablation. Overall, these data strongly suggest that targeting the myocardial mitochondria-STING-polyamine axis is a promising therapeutic strategy for cardiac hypertrophy in CKD.

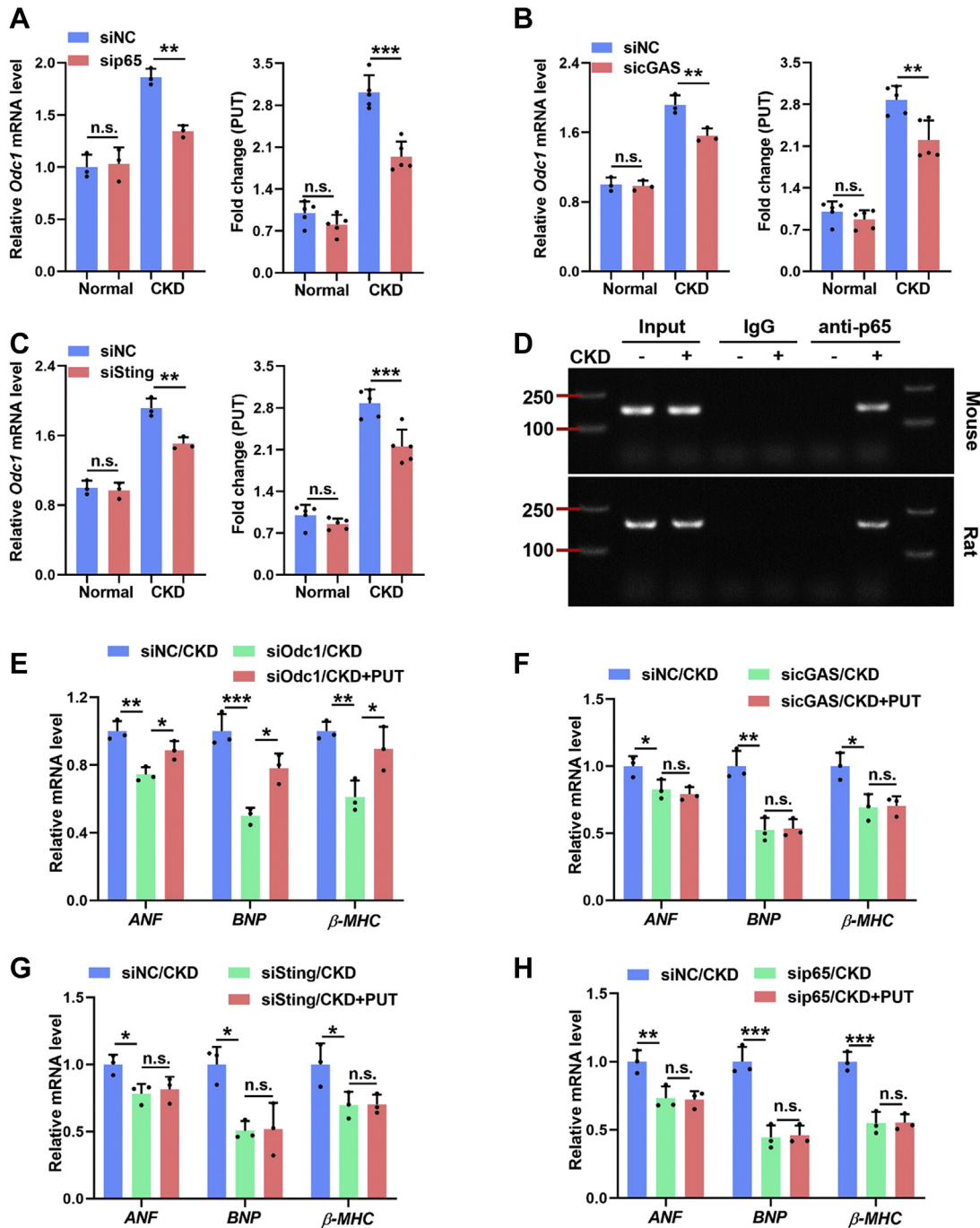
## DISCUSSION

Mitochondria are particularly rich in cardiomyocytes, and their dysfunction plays crucial roles in cardiac pathology, including CKD-associated cardiac hypertrophy.<sup>31</sup> However, the pathogenic mechanism of mitochondrial dysfunction in cardiac pathology remains largely unknown. In this study, we first reveal that mitochondrial oxidative damage is early and prominent in cardiomyocytes in a CKD milieu. Then, we identify that VDAC1 primarily mediates CKD-induced MOMP, and MOMP-mediated mtDNA release promotes the initiation of CKD-induced

### FIGURE 6 Continued

(A) The heat map shows expression profile of polyamine metabolic enzymes in the myocardia. (B) Representative WB analysis of ODC1 and GAPDH. (C) Contents of putrescine (PUT), spermidine (SPD), and spermine (SPM) in myocardia were detected using high-performance liquid chromatography. (D) Contents of PUT, SPD, and SPM in myocardia from *Odc1<sup>cko</sup>* and *Odc1<sup>fl/fl</sup>* mice with or without CKD. (E to H) Echocardiographic examination of LVIDD, LVPWD, ejection fraction, fractional shortening, and LV mass in each group. LV mass/TL ratio was calculated. (I) Representative hematoxylin and eosin staining of sagittal and midchamber sections of the hearts. Scale bar, 200 μm. (J) Relative mRNA levels of ANF, BNP, and β-MHC in myocardia from *Odc1<sup>cko</sup>* and *Odc1<sup>fl/fl</sup>* mice with or without CKD. (K to M) Echocardiographic examination of LVIDD, LVPWD, ejection fraction, fractional shortening, and LV mass in sham and CKD mice with or without PUT treatment. LV mass/TL ratio was calculated. (N) Relative mRNA levels of ANF, BNP, and β-MHC in myocardia from sham and CKD mice with or without PUT treatment. Data are represented as mean ± SD and were analyzed by 2-tailed Student's t-tests (B, C) or 1-way analysis of variance (D, F to H, J to N). n = 3 biologically independent experiments. \*P < 0.05, \*\*P < 0.01, and \*\*\*P < 0.001. Abbreviations as in Figures 1, 2, and 5.

**FIGURE 7** Myocardial ODC1-PUT Metabolic Flux Is Required for STING-NFκB Pathway-Driven Cardiac Hypertrophic Program in a CKD Milieu



(A to C) Relative mRNA levels of *Odc1* (left) and the contents of PUT (right) in NRCMs incubated with normal or CKD serum after sip65 (A), sicGAS (B), or siSting (C) treatment. (D) Binding of p65 on *Odc1* promoter was assayed using chromatin immunoprecipitation. (E) Relative mRNA levels of ANF, BNP, and β-MHC in normal and CKD serum-incubated NRCMs with siOdc1 pretreatment and PUT supplementation. (F to H) Relative mRNA levels of ANF, BNP, and β-MHC in normal and CKD serum-incubated NRCMs with sicGAS (F), siSting (G), or sip65 (H) pretreatment and PUT supplementation. Data are represented as mean ± SD and were analyzed using 1-way analysis of variance. n = 3 biologically independent experiments. n\*P < 0.05, \*\*P < 0.01, and \*\*\*P < 0.001. Abbreviations as in Figures 1, 2, and 6.

cardiac hypertrophic response via stimulation of the cGAS-STING pathway. Subsequently, the activation of myocardial NF $\kappa$ B downstream of STING drives cardiac hypertrophic program in a CKD milieu. Therefore, mitochondria serve as sentinels of the CKD milieu beyond energy production, whereas the cGAS-STING pathway serves as a switch of cardiac hypertrophic response through sensing VDAC1-mediated mtDNA release, beyond its well-known role in anti-infective responses.

Most recently, although the roles of cGAS-STING pathway in cardiac pathologies and CKD-associated accelerated atherosclerosis have been proposed,<sup>32-34</sup> its physiopathologic roles in cardiomyocytes and CKD-associated cardiac hypertrophy remain unclear. Using models of cardiomyocyte-targeted gene deletion, we show that the activation of myocardial cGAS-STING pathway intrinsically drives the cardiac hypertrophic program in a CKD milieu, arguing for a pathogenic role of the myocardial cGAS-STING pathway. Besides, NF $\kappa$ B rather than canonical IRF3 is activated by the STING in cardiomyocytes, and NF $\kappa$ B transactivates ODC1-PUT metabolic flux to facilitate the pathogenesis of cardiac hypertrophy. Therefore, although the cGAS-STING pathway as an innate immune signaling is activated in cardiomyocytes in a CKD milieu, it drives cardiac hypertrophy through a nonimmune mechanism, highlighting a distinct signal transduction of the myocardial cGAS-STING pathway during CKD-associated cardiac hypertrophy. Of note, the failure to activate IRF3 may be caused by CKD-induced p38MAPK activation in cardiomyocytes,<sup>7</sup> as p38 inhibits STING-mediated IRF3 activation.<sup>35</sup> In addition, persistent activation of the cGAS-STING pathway can also induce cell death and fibrosis,<sup>36-38</sup> which may contribute to the progression of cardiac hypertrophy to cardiac remodeling and ultimately heart failure. Altogether, these findings substantially extend our understanding of the myocardial cGAS-STING pathway in cardiac pathophysiology.

As reported, CKD can also promote cardiac hypertrophy through influencing calcium homeostasis, MAPK signaling, or NFAT signaling<sup>3,6,7</sup> or inducing pressure overload.<sup>3</sup> In fact, perturbation of calcium homeostasis will exacerbate mitochondrial oxidative damage,<sup>39</sup> whereas MAPK signaling and NFAT signaling closely interact with NF $\kappa$ B.<sup>28,40</sup> Moreover, CKD-induced activation of the mitochondria-STING-NF $\kappa$ B pathway directly induces cardiomyocyte hypertrophy without pressure overload in vitro, and myocardial ablation of STING alleviates cardiac hypertrophy with no influence on the pressure overload

**TABLE 1** Putative Binding Sequence of p65 in *Odc1* Promoter Region

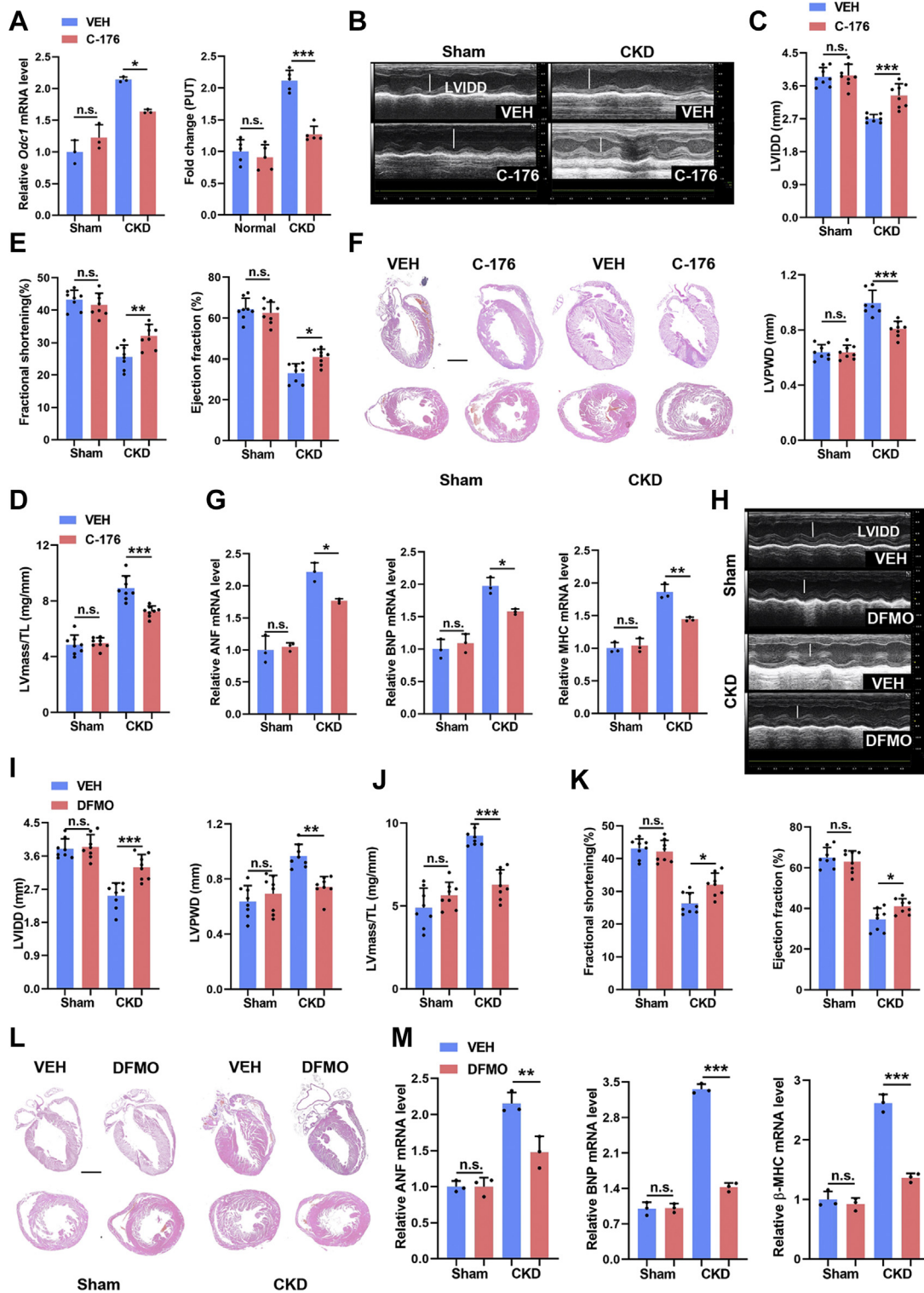
Core	Start	End	Predicated Site Sites
Mouse			
6.530	1674	1683	GGGAATACCA
6.351	876	885	GGAACATACC
Rat			
10.274	533	542	GGGACATACC
9.499	373	382	GTGGATTCC
Human			
10.833	1379	1388	GGGGCGTCCC
9.796	1097	1106	GGGACTTCCG

in CKD mice. Thus, CKD-induced activation of the myocardial mitochondria-STING-NF $\kappa$ B pathway distinctively promotes cardiac hypertrophy in CKD through a pressure overload-independent mechanism. Furthermore, although the CKD milieu changes dynamically during CKD progression, oxidative stress is a common characteristic of all stages of CKD.<sup>41</sup> Therefore, the myocardial mitochondria-STING-NF $\kappa$ B pathway may play a central role in the pathogenesis of CKD-associated cardiac hypertrophy. In contrast, other cardiac hypertrophic stimuli such as pressure overload, myocardial infarction, obesity, and diabetes are also closely associated with oxidative stress and NF $\kappa$ B activation.<sup>42</sup> On the basis of our findings, the myocardial cGAS-STING pathway-mediated sensing of mitochondrial oxidative damage may represent a common mechanism for cardiac hypertrophy.

Metabolic remodeling is also an essential molecular event in the pathogenesis of cardiac hypertrophy.<sup>26</sup> We show that myocardial ODC1-PUT metabolic flux is also implicated in the pathogenesis of CKD-associated cardiac hypertrophy. Moreover, myocardial activation of STING-NF $\kappa$ B pathway and ODC1-PUT metabolic flux are not independent but rather cooperative in the pathogenesis of CKD-associated cardiac hypertrophy, as neither of them alone can efficiently drive CKD-induced cardiac hypertrophic response. Furthermore, we also find that NF $\kappa$ B may conservatively regulate myocardial ODC1-PUT metabolic flux through transcriptional activation of ODC1. Altogether, this study unmasks an unrecognized connection between the STING-NF $\kappa$ B pathway and the polyamine metabolism and identifies NF $\kappa$ B as a coupler of hypertrophic program and polyamine metabolism in the pathogenesis of cardiac hypertrophy.

Besides, the involvement of polyamines in cardiac growth and hypertrophy has been

**FIGURE 8** Pharmacologic Inhibition of the Mitochondria-STING-Polyamine Axis Prevents Cardiac Hypertrophy in CKD



Continued on the next page

documented for decades.<sup>15</sup> Unfortunately, the feature of polyamine metabolism in cardiac pathophysiology remains undefined. We here show that myocardial ODC1-PUT metabolic flux is enhanced in CKD-induced cardiac hypertrophy, accompanied by increased expression of fetal cardiac genes. However, enhancement of myocardial ODC1-PUT metabolic flux is not merely a consequence of cardiac hypertrophy but is required to initiate CKD-induced cardiac hypertrophic response. In contrast, both the myocardial proliferation capacity and the contents of polyamines especially PUT in cardiomyocytes decline with age.<sup>43,44</sup> Therefore, ODC1-PUT metabolic flux may represent an important member of fetal cardiac metabolic profile and may be positively correlated with the proliferation potential and the pathologic hypertrophy of cardiomyocytes. As known, polyamines are highly charged aliphatic polycations that interact with nucleic acids, thereby maintaining DNA and RNA structures as well as RNA processing to affect gene expression.<sup>45</sup> It is reasonable that ODC1-PUT metabolic flux is required to reshape the gene expression program essential for cardiomyocyte proliferation and hypertrophy. Of note, although spermidine and spermine are also minorly increased in the hypertrophied cardiomyocytes, supplementation of them actually prevents cardiac hypertrophy as reported.<sup>46,47</sup> As spermidine and spermine negatively regulate ODC1-PUT metabolic flux,<sup>46,48</sup> these data further indicate a dominant role of ODC1-PUT metabolic flux in the pathogenesis of cardiac hypertrophy especially in a CKD milieu.

In addition, apart from de novo biosynthesis by ODC1, PUT can also be obtained from diet and gut microbiota.<sup>49</sup> In this study, we show that dietary PUT also facilitates the pathogenesis of cardiac hypertrophy in CKD, raising the concern about the dietary habits and symbiotic polyamine metabolism of patients with CKD. Inspiringly, chronic stimulation of innate immune sensors by microbial agents or damaged tissue as well as oxidative stress are well known to promote pathologic or malignant growth,

including hypertrophy and hyperproliferation.<sup>50</sup> Meanwhile, immunity, inflammation, and oncogenesis, wherein NF $\kappa$ B plays a central role, involve rapid cell growth and proliferation.<sup>51</sup> Our findings suggest that NF $\kappa$ B may also metabolically support these processes through rewiring the metabolic circuitry such as ODC1-PUT metabolic flux.

**STUDY LIMITATIONS.** CKD is characterized by a complex and dynamic inter-environment, with accumulation of diverse uremic toxins, deficiency of kidney-secreted soluble factors and perturbation of mineral metabolism, which may affect many other signalings. Therefore, it is necessary to identify the dominant factors that stimulate the myocardial mitochondria-STING-ODC1 axis at different stages of CKD, which are not studied here, to develop early prediction and precision therapy for CKD-associated cardiac hypertrophy. Meanwhile, future studies are needed to determine the contributions of other signalings affected by CKD milieu and their interaction with the myocardial mitochondria-STING-ODC1 axis to develop more effective therapeutic strategy for CKD-associated cardiac hypertrophy.

## CONCLUSIONS

Our findings reveal a close interaction between the STING-NF $\kappa$ B pathway and metabolic remodeling in cardiomyocytes as well as its distinct role in the pathogenesis of cardiac hypertrophy in CKD. Mitochondrial oxidative damage is an early event in response to CKD and mediates the transformation of the CKD signal to hypertrophic program through the STING-NF $\kappa$ B pathway in cardiomyocytes. In contrast, NF $\kappa$ B transcriptionally activates ODC1-PUT metabolic flux to sustain NF $\kappa$ B-driven cardiac hypertrophic program. Overall, targeting the mitochondria-STING-polyamine axis may represent a promising strategy to prevent and treat cardiac hypertrophy in patients with CKD.

**ACKNOWLEDGMENT** The authors thank Qing Zhou for excellent technical assistance.

### FIGURE 8 Continued

**(A)** Relative mRNA levels of Odc1 (**left**) and the contents of PUT (**right**) in the myocardia from sham and CKD mice with or without C-176 treatment. **(B to E)** Echocardiographic examination of LVIDD, LVPWD, ejection fraction, fractional shortening, and LV mass/TL ratio in each group. **(F)** Representative hematoxylin and eosin staining of sagittal and midchamber sections of the hearts. Scale bar, 200  $\mu$ m. **(G)** Relative mRNA levels of ANF, BNP, and  $\beta$ -MHC in myocardia from sham and CKD mice with or without C-176 supplementation. **(H to K)** Echocardiographic examination of LVIDD, LVPWD, ejection fraction, fractional shortening, and LV mass in each group. LV mass/TL ratio was calculated. **(L)** Representative hematoxylin and eosin staining of sagittal and midchamber sections of the hearts. Scale bar, 200  $\mu$ m. **(M)** Relative mRNA levels of ANF, BNP, and  $\beta$ -MHC in myocardia in each group. Data represent mean  $\pm$  SD and were analyzed using 1-way analysis of variance. n = 3 biologically independent experiments. \*P < 0.05, \*\*P < 0.01, and \*\*\*P < 0.001. DFMO = difluoromethylornithine; other abbreviations as in [Figures 1, 2, and 6](#).

## FUNDING SUPPORT AND AUTHOR DISCLOSURES

This study was supported by the Young Elite Scientist Sponsorship Program by CAST (2018QNRC001 to Dr Yang), research grants from the Key Program of the Natural Science Foundation of China (82030023 to Dr Zhao), the Natural Science Foundation of China (81874256 to Dr Du, 32171104 to Dr Yang), and the Personal Training Program for Clinical Medicine Research of Army Medical University (2018XLC1007 to Dr Zhao) and Frontier specific projects of Xinqiao Hospital (2018YQYL004 to Dr Zhao). The authors have reported that they have no relationships relevant to the contents of this paper to disclose.

**ADDRESS FOR CORRESPONDENCE:** Dr Jinghong Zhao, Department of Nephrology, Xinqiao Hospital, Army Medical University, Xinqiao Road, Chongqing 400037, China. E-mail: zhaojh@tmmu.edu.cn. OR Dr Ke Yang, Department of Nephrology, Xinqiao Hospital, Army Medical University, Xinqiao Road, Chongqing 400037, China. E-mail: jobsyangkk@163.com.

## PERSPECTIVES

**COMPETENCY IN MEDICAL KNOWLEDGE:** Cardiac hypertrophy is one of the most prevalent markers of cardiovascular disease among patients with CKD. This study for the first time reveals the pathogenic role of the myocardial mitochondria-STING-NFκB-ODC1 axis in CKD-associated cardiac hypertrophy.

**TRANSLATIONAL OUTLOOK:** Targeting the myocardial mitochondria-STING-polyamine axis holds promise for the treatment of cardiac hypertrophy in CKD. Future studies evaluating the therapeutic effect of clinically available drugs against this axis in patients with CKD will aid in the development of novel therapeutic strategies against CKD-associated cardiac hypertrophy.

## REFERENCES

1. Tonelli M, Karumanchi S, Thadhani R. Epidemiology and mechanisms of uremia-related cardiovascular disease. *Circulation*. 2016;133:518-536.
2. Wang X, Shapiro J. Evolving concepts in the pathogenesis of uraemic cardiomyopathy. *Nat Rev Nephrol*. 2019;15:159-175.
3. Faul C, Amaral A, Oskoueï B, et al. FGF23 induces left ventricular hypertrophy. *J Clin Invest*. 2011;121:4393-4408.
4. Hu M, Shi M, Cho H, et al. Klotho and phosphate are modulators of pathological uremic cardiac remodeling. *J Am Soc Nephrol*. 2015;26:1290-1302.
5. Ravid J, Kamel M, Chitalia V. Uraemic solutes as therapeutic targets in CKD-associated cardiovascular disease. *Nat Rev Nephrol*. 2021;17:402-416.
6. Touchberry C, Green T, Tchikrizov V, et al. FGF23 is a novel regulator of intracellular calcium and cardiac contractility in addition to cardiac hypertrophy. *J Physiol Endocrinol Metab*. 2013;304:E863-E873.
7. Yang K, Wang C, Nie L, et al. Klotho protects against indoxyl sulphate-induced myocardial hypertrophy. *J Am Soc Nephrol*. 2015;26:2434-2446.
8. Kolwicz S, Purohit S, Tian R. Cardiac metabolism and its interactions with contraction, growth, and survival of cardiomyocytes. *Circ Res*. 2013;113:603-616.
9. Rosca M, Tandler B, Hoppel C. Mitochondria in cardiac hypertrophy and heart failure. *J Mol Cell Cardiol*. 2013;55:31-41.
10. Dai D, Johnson S, Villarín J, et al. Mitochondrial oxidative stress mediates angiotensin II-induced cardiac hypertrophy and Galphaq overexpression-induced heart failure. *Circ Res*. 2011;108:837-846.
11. Dia M, Gomez L, Thibault H, et al. Reduced reticulum-mitochondria Ca transfer is an early and reversible trigger of mitochondrial dysfunctions in diabetic cardiomyopathy. *Basic Res Cardiol*. 2020;115:74.
12. Fernandez-Caggiano M, Kamynina A, Francois A, et al. Mitochondrial pyruvate carrier abundance mediates pathological cardiac hypertrophy. *Nat Metab*. 2020;2:1223-1231.
13. Locasale J, Cantley L. Metabolic flux and the regulation of mammalian cell growth. *Cell Metab*. 2011;14:443-451.
14. Casero R, Murray Stewart T, Pegg A. Polyamine metabolism and cancer: treatments, challenges and opportunities. *Nat Rev Cancer*. 2018;18:681-695.
15. Bartolome J, Huguenard J, Slotkin T. Role of ornithine decarboxylase in cardiac growth and hypertrophy. *Science*. 1980;210:793-794.
16. Chen M, Xin J, Liu B, et al. Mitogen-activated protein kinase and intracellular polyamine signaling is involved in TRPV1 activation-induced cardiac hypertrophy. *J Am Heart Assoc*. 2016;5:e003718.
17. Lin Y, Zhang X, Wang L, et al. Polyamine depletion attenuates isoproterenol-induced hypertrophy and endoplasmic reticulum stress in cardiomyocytes. *Cell Physiol Biochem*. 2014;34:1455-1465.
18. Tordoff M, Bachmanov A, Reed DJP. behavior. Forty mouse strain survey of water and sodium intake. *Physiol Behav*. 2007;91:620-631.
19. Chen Y, Chen Y, Shi C, et al. SOAPnuke: a MapReduce acceleration-supported software for integrated quality control and preprocessing of high-throughput sequencing data. *Gigascience*. 2018;7:1-6.
20. Li B, Dewey CN. RSEM: accurate transcript quantification from RNA-Seq data with or without a reference genome. *BMC Bioinformatics*. 2011;12:323.
21. Sabrane K, Kruse M, Fabritz L, et al. Vascular endothelium is critically involved in the hypotensive and hypovolemic actions of atrial natriuretic peptide. *J Clin Invest*. 2005;115:1666-1674.
22. Galluzzi L, Kepp O, Kroemer G. Mitochondria: master regulators of danger signalling. *Nat Rev Mol Cell Biol*. 2012;13:780-788.
23. Bock F, Tait S. Mitochondria as multifaceted regulators of cell death. *Nat Rev Mol Cell Biol*. 2020;21:85-100.
24. Kim J, Gupta R, Blanco L, et al. VDAC oligomers form mitochondrial pores to release mtDNA fragments and promote lupus-like disease. *Science*. 2019;366:1531-1536.
25. Hopfner K, Hornung V. Molecular mechanisms and cellular functions of cGAS-STING signalling. *Nat Rev Mol Cell Biol*. 2020;21:501-521.
26. Nakamura M, Sadoshima J. Mechanisms of physiological and pathological cardiac hypertrophy. *Nat Rev Cardiol*. 2018;15:387-407.
27. Gordon J, Shaw J, Kirshenbaum L. Multiple facets of NF-κB in the heart: to be or not to NF-κB. *Circ Res*. 2011;108:1122-1132.
28. Liu Q, Chen Y, Auger-Messier M, Molkenin J. Interaction between NFκB and NFAT coordinates cardiac hypertrophy and pathological remodeling. *Circ Res*. 2012;110:1077-1086.
29. Zhao Q, Viswanadhapalli S, Williams P, et al. NADPH oxidase 4 induces cardiac fibrosis and hypertrophy through activating Akt/mTOR and NFκB signaling pathways. *Circulation*. 2015;131:643-655.
30. Haag S, Gulen M, Reymond L, et al. Targeting STING with covalent small-molecule inhibitors. *Nature*. 2018;559:269-273.
31. Juni R, Al-Shama R, Kuster D, et al. Empagliflozin restores chronic kidney disease-induced impairment of endothelial regulation of cardiomyocyte relaxation and contraction. *Kidney Int*. 2021;99:1088-1101.

32. Gong Y, Li G, Tao J, et al. Double knockout of Akt2 and AMPK accentuates high fat diet-induced cardiac anomalies through a cGAS-STING-mediated mechanism. *Biochim Biophys Acta Mol Basis Dis.* 2020;1866:165855.
33. Wang S, Wang L, Qin X, et al. ALDH2 contributes to melatonin-induced protection against APP/PS1 mutation-prompted cardiac anomalies through cGAS-STING-TBK1-mediated regulation of mitophagy. *Signal Transduct Target Ther.* 2020;5:119.
34. Zhang Y, Chen W, Wang Y. STING is an essential regulator of heart inflammation and fibrosis in mice with pathological cardiac hypertrophy via endoplasmic reticulum (ER) stress. *Biomed Pharmacother.* 2020;125:110022.
35. Chen Y, Wang L, Jin J, et al. p38 inhibition provides anti-DNA virus immunity by regulation of USP21 phosphorylation and STING activation. *J Exp Med.* 2017;214:991-1010.
36. Chung K, Dhillon P, Huang S, et al. Mitochondrial damage and activation of the STING pathway lead to renal inflammation and fibrosis. *Cell Metab.* 2019;30:784-799.e5.
37. Luo W, Wang Y, Zhang L, et al. Critical role of cytosolic DNA and its sensing adaptor STING in aortic degeneration, dissection, and rupture. *Circulation.* 2020;141:42-66.
38. Luo X, Li H, Ma L, et al. Expression of STING is increased in liver tissues from patients with NAFLD and promotes macrophage-mediated hepatic inflammation and fibrosis in mice. *Gastroenterology.* 2018;155:1971-1984.e4.
39. Bertero E, Maack C. Calcium signaling and reactive oxygen species in mitochondria. *Circ Res.* 2018;122:1460-1478.
40. Schulze-Osthoff K, Ferrari D, Riehemann K, Wesselborg S. Regulation of NF-kappa B activation by MAP kinase cascades. *Immunobiology.* 1997;198:35-49.
41. Dounousi E, Papavasiliou E, Makedou A, et al. Oxidative stress is progressively enhanced with advancing stages of CKD. *Am J Kidney Dis.* 2006;48:752-760.
42. Ramachandra C, Cong S, Chan X, et al. Oxidative stress in cardiac hypertrophy: From molecular mechanisms to novel therapeutic targets. *Free Radic Biol Med.* 2021;166:297-312.
43. Nisenberg O, Pegg A, Welsh P, et al. Overproduction of cardiac S-adenosylmethionine decarboxylase in transgenic mice. *Biochem J.* 2006;393:295-302.
44. Wang W, Li L, Xia X, et al. Dedifferentiation, proliferation, and redifferentiation of adult mammalian cardiomyocytes after ischemic injury. *Circulation.* 2017;136:834-848.
45. Sánchez-Jiménez F, Medina M, Villalobos-Rueda L, et al. Polyamines in mammalian pathophysiology. *Cell Mol Life Sci.* 2019;76:3987-4008.
46. Eisenberg T, Abdellatif M, Schroeder S, et al. Cardioprotection and lifespan extension by the natural polyamine spermidine. *Nat Med.* 2016;22:1428-1438.
47. Madeo F, Eisenberg T, Pietrocola F, Kroemer G. Spermidine in health and disease. *Science.* 2018;359:eaan2788.
48. Pegg A. Regulation of ornithine decarboxylase. *J Biol Chem.* 2006;281:14529-14532.
49. Ramos-Molina B, Queipo-Ortuño M, Lambertos A, et al. Dietary and gut microbiota polyamines in obesity- and age-related diseases. *Front Nutr.* 2019;6:24.
50. Greten F, Grivnennikov S. Inflammation and cancer: triggers, mechanisms, and consequences. *Immunity.* 2019;51:27-41.
51. Taniguchi K, Karin M. NF-κB, inflammation, immunity and cancer: coming of age. *Nat Rev Immunol.* 2018;18:309-324.

---

**KEY WORDS** cardiac hypertrophy, cGAS-STING pathway, chronic kidney disease, mitochondria, polyamine metabolism

---

**APPENDIX** For supplemental figures, tables, and tests of normality, please see the online version of this paper.